Capability of a regional climate model to simulate climate variables requested for water balance computation: a case study over northeastern France

Damien Boulard, Thierry Castel, Pierre Camberlin, Anne-Sophie Sergent, Nathalie Bréda, Vincent Badeau, Aurélien Rossi, Benjamin Pohl

To cite this version:

Damien Boulard, Thierry Castel, Pierre Camberlin, Anne-Sophie Sergent, Nathalie Bréda, et al.. Capability of a regional climate model to simulate climate variables requested for water balance computation: a case study over northeastern France. Climate Dynamics, 2016, 46 (9-10), pp.2689-2716. 10.1007/s00382-015-2724-9 . hal-01309572

HAL Id: hal-01309572
https://hal.science/hal-01309572v1

Submitted on 10 Nov 2022

Capability of a regional climate model to simulate climate variables requested for water balance computation: a case study over northeastern France

Damien Boulard[1], Thierry Castel[1,2], Pierre Camberlin[1], Anne-Sophie Sergent[3,4], Nathalie Bréda[3], Vincent Badeau[3], Aurélien Rossi[1], Benjamin Pohl[1]

Abstract This paper documents the capability of the ARW/WRF regional climate model to regionalize near-surface atmospheric variables at high resolution (8 km) over Burgundy (northeastern France) from daily to interannual timescales. To that purpose, a 20-year continuous simulation (1989–2008) was carried out. The WRF model driven by ERA-Interim reanalyses was compared to in situ observations and a mesoscale atmospheric analyses system (SAFRAN) for five near-surface variables: precipitation, air temperature, wind speed, relative humidity and solar radiation, the last four variables being used for the calculation of potential evapotranspiration (ET_0). Results show a significant improvement upon ERA-Interim. This is due to a good skill of the model to reproduce the spatial distribution for all weather variables, in spite of a slight over-estimation of precipitation amounts mostly during the summer convective season, and wind speed during winter. As compared to the Météo-France observations, WRF also improves upon SAFRAN analyses, which partly fail at showing realistic spatial distributions for wind speed, relative humidity and solar radiation—the latter being strongly underestimated. The SAFRAN ET_0 is thus highly under-estimated too. WRF ET_0 is in better agreement with observations. In order to evaluate WRF's capability to simulate a reliable ET_0, the water balance of thirty Douglas-fir stands was computed using a process-based model. Three soil water deficit indexes corresponding to the sum of the daily deviations between the relative extractible water and a critical value of 40 % below which the low soil water content affects tree growth, were calculated using the nearest weather station, SAFRAN analyses weather data, or by merging observation and WRF weather variables. Correlations between Douglas-fir growth and the three estimated soil water deficit indexes show similar results. These results showed through the ET_0 estimation and the relation between mean annual SWDI and Douglas-fir growth index that the main difficulties of the WRF model to simulate soil water deficit is mainly attributable to its precipitation biases. In contrast, the low discrepancies between WRF and observations for air temperature, wind speed, relative humidity and solar radiation make then usable for the water balance and ET_0 computation.

Keywords Regional climate modelling · WRF · Potential evapo-transpiration · Water balance · Soil water deficit · Douglas-fir

1 Introduction

In the context of anthropogenic climate change, it is widely recognized that many sectors will be affected by water deficits in different components of the land surface hydrological cycle. In particular, any change in the soil water balance will have major consequences for plant growth. An increase of the frequency and intensity of soil drought events is expected in the northern hemisphere, especially during spring and summer (IPCC 2007). During the 2003

✉ Damien Boulard
damien.boulard@u-bourgogne.fr

[1] Centre de Recherches de Climatologie, UMR 6282 Biogéosciences, CNRS/Université de Bourgogne Franche-Comté, 6 Boulevard Gabriel, 21000 Dijon, France

[2] Département Agronomie-Environnement, AgroSup, 21000 Dijon, France

[3] UMR 1137 Ecologie et Ecophysiologie Forestières, INRA, 54280 Champenoux, France

[4] UMR 1137 Ecologie et Ecophysiologie Forestières, Université de Lorraine, BP 239, 54506 Vandoeuvre les Nancy, France

drought and heat-wave episode, coniferous species such as Douglas-fir presented visual symptoms like abnormal coloration, needle loss or dead branches followed by adverse effects such as decline and tree mortality (Sergent et al. 2012). Over northeastern France, recent projections using the Weather Research and Forecast (WRF) regional climate model (RCM) of the SRES-A2 scenario have shown a warming of up to 3 °C for 2030–2050 and 5 °C by the end of the century (Xu et al. 2012). Thus, the 2003 episode should not be considered as an exceptional extreme event, but as an example of forthcoming forest-impacting hazards in a near future (Bréda et al. 2006; Betsch et al. 2010).

Assessing impacts of climate variability on the water balance requires reliable observation data representative of a given geographical area but usually unavailable at fine scales. Precipitation and potential evapotranspiration (ET_0) are two elements with a major role in the hydrological cycle and soil water balance. The FAO-56 Penman–Monteith (PM) equation (Allen et al. 1998) has been proposed as a worldwide standard by the Food and Agriculture Organisation (FAO) of the United Nations due to its accuracy to evaluate ET_0 at different time-scales. However, the PM equation requires numerous meteorological variables: air temperature, wind speed, relative humidity and solar radiation. Several authors highlighted the problem of the data availability due to the scarcity of in situ weather variables measurements (Shih et al. 1983; Remesan et al. 2008) and proposed simplified empirical methods (Droogers and Allen 2002; Pereira 2004; Gavilan et al. 2006), which vary in complexity and data requirements.

Adaptation to climate change relies on sustainable water resource management that requires projections, at high spatial and temporal resolutions, of all climate variables involved in water balance computation. Globally assimilated data such as the European Centre for Medium-Range Weather Forecasts (ECMWF) reanalyses, or general circulation model (GCM) simulations, can compensate for the lack of available data. But their coarse spatial resolution (typically 80–250 km) is irrelevant and prevents them from being used directly for local impact studies or extreme events reconstruction (Zorita and Von Storch 1999). Impact models often need input climatic data at a resolution finer than 10 km and require thus a downscaling step to derive high-resolution information (Boé et al. 2007). During the last decade, an increasing number of studies assessed the usefulness and limitations associated with the dynamical downscaling of low-resolution GCM output using regional climate models (RCM: Giorgi and Mearns 1991; Laprise 2008; Landman et al. 2009; Rummukainen 2010). Such numerical dynamic regionalization of large-scale climate data has been carried out for many parts of the world, in the framework of international programs such as, among others, PRUDENCE (Christensen and Christensen 2007) or ENSEMBLES (Van der Linden and Mitchell 2009) and more recently CORDEX (e.g., Jones et al. 2011), producing thus high-resolution climate simulations of atmosphere and land. The methodology consists in forcing laterally a high-resolution atmospheric model with coarser-resolution GCM output, usually without feedback to the parent solution. RCM experimental protocols assume that the region of interest (1) is influenced by atmospheric variability patterns that are of larger spatial extension than the simulated domain; (2) is passive, i.e. it is influenced by large-scale modes of variability without modifying their development, life cycle, and intrinsic properties in return (Boulard et al. 2013).

In this study, we propose to examine the capability of a current state-of-the-art RCM to downscale the coarse global reanalyses into higher resolution data, and simulate near-surface atmospheric spatial and temporal variability of weather variables used in the computation of potential evapotranspiration (ET_0) and water balance. Compared to precipitation and temperature, there has been relatively little work attempting to assess the skill of an RCM dynamical downscaling of these variables (Frey-Buness et al. 1995; Copeland et al. 1996; Heck et al. 2001; Correia et al. 2007; Boé et al. 2007; Ishak et al. 2010), partly due to the lack of representative high-resolution observational data. Consequently, there is also a lack of data quality verification and sensitivity analysis regarding downscaled data in the hydrological community (Ishak et al. 2010). Actually, higher resolution does not guarantee improved RCM outputs, hence the necessity for preliminary quality assessment before using such data for impact studies (e.g., water balance computation).

The non-hydrostatic Weather Research and Forecast (WRF) model (Skamarock et al. 2008) has been already successfully applied over northeastern France, for temperature and precipitation downscaling (Xu et al. 2012; Marteau et al. 2014). Temperature and precipitation are generally the most relevant and best studied meteorological variables for hydrological impact studies (Maraun et al. 2010). It is already known that precipitation simulated by RCMs is highly sensitive to their physics and usually show larger biases than surface temperature. Precipitation amounts are among the most sensitive quantities to the physical package. Their geography, intensity, and intraseasonal characteristics are predominantly sensitive to various physical schemes, including parameterizations for atmospheric convection, planetary boundary layer and cloud microphysics (Crétat et al. 2012). A previous study (Castel et al. 2010) also shows that the overestimation of precipitation amounts is significantly reduced by an improvement of the Land-Use/Land-Cover data used to perform the simulation. Over northeastern France, surface data taken from the Moderate Resolution Imaging Spectroradiometer (MODIS) allows to better represent the surface albedo and latent heat flux involved in the simulation of precipitation than the United States Geological Survey data.

In the present work, the WRF model is used to perform high-resolution (8 km) simulations over the Burgundy region (northeastern France) at a daily time-step for the period 1989–2008. Here, both the downscaled data and original forcing reanalyses (namely, ERA-Interim) are compared to the mesoscale SAFRAN analyses ("Système d'Analyse Fournissant des Renseignements Atmosphériques à la Neige", Durand et al. 1993; Durand 1995), which are already used by hydrological and agro-forestry communities (Boé et al. 2007; Durand et al. 2009). In France, operational systems such as SAFRAN provide high resolution gridded atmospheric data assessed at the national scale (Quintana-Seguí et al. 2008; Vidal et al. 2010). In order to quantify RCM-produced biases, the SAFRAN mesoscale reanalysis can be used as a reference (Szczypta et al. 2011). The estimated ET_0 is also verified with the corresponding ground-based observed data available over the region.

Downscaled climatic data are next used as input data for a process-based model (Biljou©: Granier et al. 1999) to simulate the water balance of thirty Douglas-fir stands across Burgundy. Douglas-fir, used as a plantation tree for timber in several upland parts of the region, is a species highly sensitive to soil water deficit (Sergent et al. 2012). Among the process-based models, the daily water balance model Biljou© is dedicated to forest stands, and allows to calculate each component of the water flux (tree transpiration, understorey evapo-transpiration, rainfall interception, drainage) and the daily soil water content under forests. The model quantifies the intensity, the duration and the frequency of drought experienced by the stand. It has already been successfully applied to different stands (Bréda et al. 2006; Gandois et al. 2010; Van der Heijden et al. 2011; Michelot et al. 2012) and over parts of Burgundy (Sergent et al. 2012; Van der Heijden et al. 2013).

This study aims at (1) documenting how accurately the WRF model is capable to reproduce the spatial and temporal variability of 2 m-air temperature, relative humidity, 2 m-wind speed, solar radiation, precipitation and potential evapotranspiration; (2) quantifying the RCM skills and weaknesses to simulate the water balance, based on a daily lumped water balance model for forests. The ability of the RCM to provide skillful input data for water balance computation will be assessed by focusing on the soil water deficits obtained from Biljou©.

This paper is organized as follows. Section 2 presents the data used and the experimental setup. Section 3 evaluates the capability of the regional model in simulating air temperature, wind speed, relative humidity and solar radiation variability and spatial distribution over Burgundy. Section 4 focuses on precipitation and ET_0 used for the computation of the water balance. Results are finally summarized and discussed in Sect. 5.

2 Data and experimental setup

2.1 Study area

Burgundy is a region located in northeastern France. It is composed by the Yonne, Nièvre, Côte d'Or and Saône-et-Loire departments (Fig. 1a—D03) and covers an area of 31,528 km^2. It is characterized by a relatively complex topography, surrounded by the Jura and Alps massifs on the East, and the Massif Central on the Southwest. The topography is mainly characterized by two alluvial plains in the Northwest (Paris basin) and in the Southeast (Saône tectonic trough), rolling hills (maximal elevation of 901 m in the Morvan massif—Fig. 1b) and plateaux running from North to South across the central parts of the region. The highly fragmented land-use is dominated by pastures and croplands (2,000,000 ha, 64.3 %), forests (970,000 ha, 30 %) and vineyards (30,000 ha, 1 %). The climate of Burgundy is predominantly semi-continental with relatively short, warm summers and cool winters.

2.2 Experimental setup

The present study uses the WRF model (Skamarock et al. 2008) version 3.1.1. WRF is a non-hydrostatic model, suitable for simulating a wide range of scales, from thousands of kilometres to a few meters, with a large number of available options in what concerns the model core and physical parameterizations, making it appropriate for numerical prediction and climate simulation. WRF was setup with 3 two-way nested domains with respectively, 120.0, 32.5 and 8.2 km horizontal grid spacing and 28 sigma levels on the vertical (Fig. 1a). Lateral forcing is provided every 6-hours by ECMWF ERA-Interim reanalyses (Berrisford et al. 2009; Dee et al. 2011), from 1000 to 10 hPa (18 vertical levels) at a 1.5° horizontal resolution. ERA-Interim reproduces observed climate more realistically than other reanalysis products such as ERA-40 or NNRP-1 (Mooney et al. 2010), a result supported over France by the recent verifications by Szczypta et al. (2011). The ERA-Interim reanalyses are generated by an a posteriori integration of the Integrated Forecasting System atmospheric GCM with 6 hourly four-dimensional assimilations of satellite data, buoys and radiosondes, at a T255 spectral truncation with 60 vertical levels.

WRF integration time-step is fixed at 150 s and data are archived every 6 h over 1989–2008, after a 1-year-long spin-up. The 3rd inner domain extending from 45.91 to 48.52°N and 2.58 to 5.62°E, covers Burgundy and adjacent

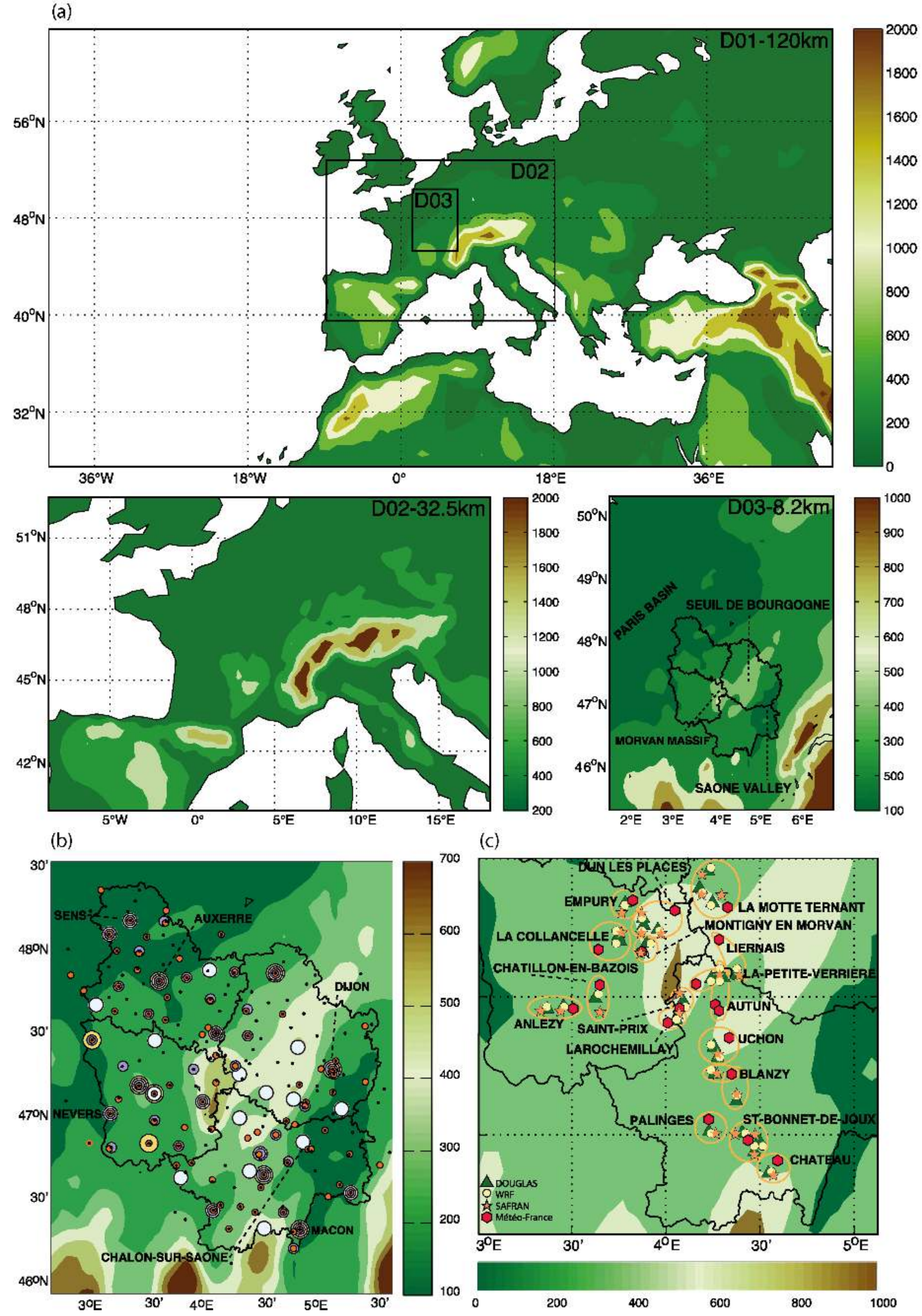

(a)
D01-120km
D02
D03
56°N
48°N
40°N
32°N
36°W
18°W
0°
18°E
36°E
2000
1800
1600
1400
1200
1000
800
600
400
200
0
D02-32.5km
51°N
48°N
45°N
42°N
5°W
0°
5°E
10°E
15°E
D03-8.2km
50°N
49°N
48°N
47°N
46°N
2°E
3°E
4°E
5°E
6°E
PARIS BASIN
SEUIL DE BOURGOGNE
MORVAN MASSIF
SAONE VALLEY
1000
900
800
700
600
500
400
300
100
(b)
SENS
AUXERRE
DIJON
NEVERS
MACON
CHALON-SUR-SAONE
48ON
47ON
46ON
30'
3OE
4OE
5OE
700
600
500
400
300
200
100
(c)
DUN LES PLACES
EMPURY
LA MOTTE TERNANT
MONTIGNY EN MORVAN
LA COLLANCELLE
LIERNAIS
CHATILLON-EN-BAZOIS
LA-PETITE-VERRIERE
AUTUN
ANLEZY
SAINT-PRIX
LAROCHEMILLAY
UCHON
BLANZY
PALINGES
ST-BONNET-DE-JOUX
CHATEAU
DOUGLAS
WRF
SAFRAN
Météo-France
3OE
30'
4OE
5OE
0
200
400
600
800
1000

◀ **Fig. 1** **a** Settings and orography (m) of the three nested WRF domains. *Colors* show the corresponding topography such as is appears in WRF grids. **b** Location of Météo-France stations. *Colored circles* permit to differentiate stations that record precipitation (*black*), temperature (*red*), wind speed (*light blue*), relative humidity (*purple*) and solar radiation (*yellow*). **c** Location of Douglas-fir stands and associated weather stations (Météo-France)

territories, at an 8 km horizontal resolution (58 × 67 grid points). A similar domain has been successfully used in several previous modelling studies of the climate variability of Burgundy (Castel et al. 2010; Marteau et al. 2014), and a climate change regionalization exercise (Xu et al. 2012). The physical package includes the Kain-Frisch cumulus scheme (Kain 2004), the Morrison scheme cloud microphysics (Morrison et al. 2009), and the Yonsei University planetary boundary layer (Hong et al. 2006). Radiative transfers are parameterized with the Rapid Radiative Transfer Model Scheme (Mlawer et al. 1997) for long-waves and the Dudhia (1989) scheme for short waves. Surface data are taken from the Moderate Resolution Imaging Spectroradiometer (MODIS, Friedl et al. 2002) databases, which comprise a 20-category land-use index. Over landmasses, WRF is coupled with the 4-layer NOAH land surface model (Chen and Dudhia 2001). Soil moisture, which is one of the key parameters that control surface energy partition and water budget, is initialized from the ERA-Interim data. The four (10, 30, 60, and 100 cm) layers of the NOAH model are interpolated from the four ERA-Interim layers (7, 28, 100 and 255 cm depth) of soil moisture and temperature data. Sea surface temperatures are prescribed every 6 h by linear interpolation of monthly ERA-Interim sea surface temperatures. The lateral buffer zone used to smooth the relaxation of the model toward the prescribed atmospheric forcing is made of five grid points (1 grid point of forcing plus 4 grid points of relaxation).

2.3 Data

The assessment of the WRF simulation is done by comparison with four datasets: (1) weather station records of the Météo-France Weather Station Network (MWSN), (2) 8 km-gridded SAFRAN analyses, (3) gridded SATMOS (Service d'Archivage et de Traitement Météorologique des Observations Spatiales) data and (4) the raw ERA-Interim reanalyses.

MWSN daily weather station records provide the observed near-surface weather data over the period 1989–2008 (Fig. 1b). The stations are located in several different terrain situations with a variety of Land-Use/Land-Cover patterns such as forests, croplands, and urban areas. Daily records from 127 rain gauges are extracted from the MWSN. The observed air temperature is derived from 89 weather stations. Both of these datasets show a homogenous spatial distribution and no missing values. Annual and monthly means (totals) of temperature (precipitation) are interpolated onto a 1 km resolution grid using a three-dimensional (latitude, longitude, elevation) thin plate splines method with altitude as covariate (Hutchinson 1995). Anomalies, defined as the departure from the monthly mean (total) temperature (precipitation), are interpolated onto the same grid and combined with the monthly mean grid. Observed records of solar net radiation, wind speed and relative humidity are available for 9, 28 and 36 weather stations respectively. These variables have ~30 % of missing values, mostly in the early part of the records, and which were not reconstructed. For these variables, due to the scarcity and heterogeneous distribution of weather stations, comparisons are done using the nearest WRF grid-point. Estimated Météo-France ET_0 data are computed for 24 weather stations over the period 2004–2008 using the Penman–Monteith equation over a hypothetic grass reference crop surface; they include some missing values too.

To overcome the scarcity of observed solar radiation data, solar radiation maps are derived from the visible channel of the Météosat satellite following the Gautier et al. (1980) method. These maps are provided by the SATMOS service over the period 1996–2006 at a 10-days time-step and a resolution of 10 km. The sensitivity of the visible radiometer is assessed following the observed inter-annual variability in a homogeneous desert environment. The results are compared every month to pyranometric records from the MWSN (42 stations) across France.

Cell to cell comparison with the gridded high-resolution SAFRAN analyses is performed after a simple nearest neighbour interpolation. SAFRAN is a mesoscale atmospheric analyses system, which produces surface atmospheric variables covering France on a regular grid at an 8 km resolution using observations from the automatic, synoptic, and climatologic MWSN networks, and ECMWF reanalyses (Szczypta et al. 2011). Analyses are made on 615 climatically homogenous zones taking topography effects into account. Vertical profiles of temperature, humidity, wind speed and cloudiness are interpolated at the hourly time-step by combining an optimal interpolation every 6 h, and a variational interpolation over 6 h windows (Durand et al. 2009). Precipitation analysis is performed daily. The solar radiation is calculated using a radiative transfer scheme (Vautard et al. 2013). Quintana-Seguí et al. (2008) and Vidal et al. (2010) already assessed the quality of SAFRAN analyses over France and highlighted that the increasing number of ground observations improves its realism over time. Hence, solar radiation and wind speed are the variables most affected by the scarcity of observations.

2.4 Potential evapotranspiration estimates

Potential evapotranspiration over a grass reference surface is estimated using FAO-56 Penman–Monteith (PM) equation. The reliability of PM equation (Allen et al. 1998) has been assessed by numerous authors (Allen et al. 1989; Bell et al. 2011; Prudhomme and Williamson 2013; McAfee 2013). The PM equation ranked as the best method for all climatic conditions. This method combines energy balance and mass transfer concepts (Penman 1948) with stomatal and surface resistance (Monteith 1981). ET_0 is dependent on four primary climatological parameters, namely solar radiation, wind speed, humidity and air temperature (Allen et al. 1998). For WRF simulation and SAFRAN analyses, the PM equation is expressed as:

$$\mathrm{ET}_0 = \frac{0.408\Delta(R_\mathrm{n} - G) + \gamma \frac{900}{T+273} u_2 (e_\mathrm{s} - e_\mathrm{a})}{\Delta + \gamma(1 + 0.34 u_2)} \tag{1}$$

where ET_0 = reference evapotranspiration (mm day^{-1}), R_n = net radiation at the crop surface (MJ m^{-2} day^{-1}), G = soil heat flux density (considered as $G \approx 0$ MJ m^{-2} day^{-1}), T = air temperature at 2 m height (°C), u_2 = wind speed at 2 m height (m s^{-1}), e_s = saturation vapour pressure (kPa), e_a = actual vapour pressure (kPa), e_s–e_a = saturation vapour pressure deficit (kPa), Δ = slope vapour pressure curve (kPa $°C^{-1}$), γ = psychrometric constant (kPa $°C^{-1}$).

Xu and Singh (2001) found that wind speed (temperature and relative humidity) exerts more control on ET_0 at hourly (longer) time scales.

2.5 Soil water deficit and Douglas-fir growth index

Douglas-fir (*Pseudotsuga menziesii*) was chosen due to the high sensitivity of its radial growth to soil water deficit events. Data from thirty Douglas-fir planted stands (Fig. 1c) are used to evaluate WRF´s capability to simulate a reliable ET_0, which can be used in forest dendroecology studies. For each stand, annual soil water deficit indexes were calculated using the MWSN and/or WRF weather variables. Resulting soil water deficit indexes were compared and correlated to an annual radial growth index.

Stand and soil properties, and annual growth index taking into account tree age were obtained from a dendroecological study of Douglas-fir decline induced by extreme and recurrent soil water deficit (Sergent et al. 2012). Field observation and tree coring were performed during March to April 2009. At each site, a dendroecological plot with a radius of 15 m (700 m^2) was established, avoiding edge and gaps. A soil pit was dug to describe the soil profile to calculate extractable soil water. Diameter at breast height, dominant height, and crown condition were also recorded to characterize the dendrometry of each stand. Sapwood width was measured in the cores and sapwood area was estimated from diameter at breast height. Tree leaf area was derived from sapwood area with an allometric relationship. 15 trees per stand were cored to the pith to evaluate tree age and calculate an annual radial growth index. Basal area increment was computed from ring width and used to characterise radial growth. The mean annual basal area increment was calculated for each plot. To allow growth comparison between plots of different ages, all series were standardised. Final chronologies at the plot level were prepared by averaging the annual residuals to yield a growth index (GI) expressed as a percent of the expected growth under average conditions, see Sergent et al. (2012) for more details.

Soil water deficit was computed using the daily lumped water balance model for forests Biljou© (Granier et al. 1999). Biljou© (https://appgeodb.nancy.inra.fr/biljou/) is a process-based model, which calculates water fluxes (interception, transpiration, actual evapotranspiration, drainage) and soil water content at a daily time-step. The model computes potential evapo-transpiration according to the Penman equation with forest albedo. For each stand, Biljou© quantifies soil parameters (maximum extractable water, bulk density, and water content at permanent wilting point for each soil layer) and stand parameters (leaf area index, fine root distribution). Soil water shortage has an impact on stomatal regulation as soon as Relative Extractable Water (REW) in the soil drops below a critical value of 40 % (Granier et al. 1999). Day-by-day computation of soil water content includes temporal autocorrelation, as REW is never reinitialised. The soil water deficit index (SWDI) calculated by Biljou© corresponds to the sum of the daily deviations between the relative extractible water and the critical value of 40 %.

The relationship between mean annual intensity of soil water deficit calculated with MWSN and/or WRF elementary variables (global radiation, wind speed, air temperature, relative humidity to compute ET_0-Penman and rainfall) and mean annual growth index was examined using a linear regression for the period 1989–2008.

3 Analysis of potential evapotranspiration components

This section presents the results (summarized in Table 1) obtained for each atmospheric variable used to estimate ET_0 (namely, air temperature, relative humidity, wind speed, solar radiation). Comparisons are performed between WRF

Table 1 WRF mean, bias, RMSE and R^2 against MWSN observations over the period 1989–2008 (2004–2008 for ET_0)

Month	Mean	Bias	RMSE	r^2	Mean	Bias	RMSE	r^2
	Temperature °C				Incoming solar radiation j cm^{-2}			
Jan	3.81	0.27	0.95	0.73	351.40	−1.16	57.93	0.11
Feb	3.92	−0.63	0.98	0.94	617.00	−4.50	99.40	0.19
Mar	6.67	−1.04	1.27	0.76	982.90	−96.69	129.31	0.62
Apr	8.90	−1.01	1.25	0.69	1431.60	−53.41	156.72	0.69
May	14.29	−0.29	0.73	0.80	2002.60	101.82	198.72	0.25
Jun	17.47	−0.09	0.85	0.71	2350.50	255.29	282.88	0.51
Jul	19.87	0.05	0.85	0.79	2323.50	249.45	281.69	0.26
Aug	19.79	0.01	1.10	0.57	1857.10	74.82	113.45	0.67
Sep	15.39	−0.19	0.63	0.86	1228.40	−73.71	130.77	0.49
Oct	11.75	−0.23	0.79	0.85	763.70	−0.14	85.64	0.31
Nov	6.46	−0.03	0.73	0.84	401.60	−12.72	60.48	0.32
Dec	3.91	0.23	0.99	0.78	297.70	19.00	39.27	0.59
Year	11.07	−0.24	0.61	0.99	1220.80	38.62	147.74	0.97
	Relative humidity %				Precipitation mm day^{-1}			
Jan	85.61	−0.29	2.81	0.43	2.22	0.13	0.51	0.80
Feb	83.09	1.50	4.11	0.26	2.38	0.21	0.73	0.63
Mar	79.84	4.80	6.52	0.17	2.33	0.45	0.69	0.82
Apr	75.87	2.86	5.12	0.75	3.06	0.60	0.99	0.66
May	76.91	3.83	4.78	0.19	3.53	1.15	1.48	0.58
Jun	75.24	3.01	4.74	0.24	2.92	0.74	1.10	0.25
Jul	70.16	0.84	4.11	0.12	2.58	0.35	0.83	0.28
Aug	67.41	−2.59	4.69	0.57	2.37	0.20	0.86	0.41
Sep	71.60	−4.75	6.21	0.34	2.45	0.06	0.94	0.46
Oct	78.38	−4.38	5.14	0.53	2.45	−0.22	0.67	0.63
Nov	84.59	−2.19	4.30	0.22	2.59	−0.15	0.69	0.76
Dec	86.14	−0.82	2.90	0.46	2.76	0.47	0.78	0.70
Year	77.87	0.14	3.56	0.73	2.64	0.33	1.01	0.47
	Wind speed m s^{-1}				ET_0 mm day^{-1}			
Jan	3.18	0.94	0.98	0.84	0.63	0.07	0.06	0.72
Feb	3.24	0.72	0.77	0.84	0.85	−0.06	0.15	0.84
Mar	3.20	0.55	0.58	0.87	1.35	−0.20	0.37	0.16
Apr	3.12	0.48	0.54	0.40	2.07	−0.44	0.48	0.91
May	2.69	0.52	0.56	0.54	3.17	−0.10	0.23	0.70
Jun	2.53	0.41	0.49	0.14	3.98	−0.22	0.41	0.46
Jul	2.52	0.36	0.41	0.60	4.33	−0.25	0.31	0.93
Aug	2.37	0.22	0.28	0.52	3.65	0.25	0.17	0.89
Sep	2.45	0.54	0.58	0.63	2.35	−0.15	0.29	0.22
Oct	2.70	0.85	0.87	0.62	1.46	0.01	0.21	0.94
Nov	2.83	0.90	0.95	0.56	0.74	0.09	0.08	0.80
Dec	3.19	0.86	0.91	0.69	0.56	0.15	0.06	0.91
Year	2.57	0.61	0.69	0.66	2.10	−0.07	0.37	0.94

All statistics were calculated using analyzed values for each point at the daily time-step

simulated variables and the ERA-Interim, SAFRAN and MWSN data sets over the period 1989–2008. The aim of this section is to evaluate the capability of the WRF model to downscale the ERA-Interim data at a high spatial resolution appropriate for impact studies.

3.1 Temperature

Figure 2 shows the climatological annual mean 2 m-temperature simulated by WRF (a), estimated by SAFRAN (b) and measured by the MWSN stations (c), together with

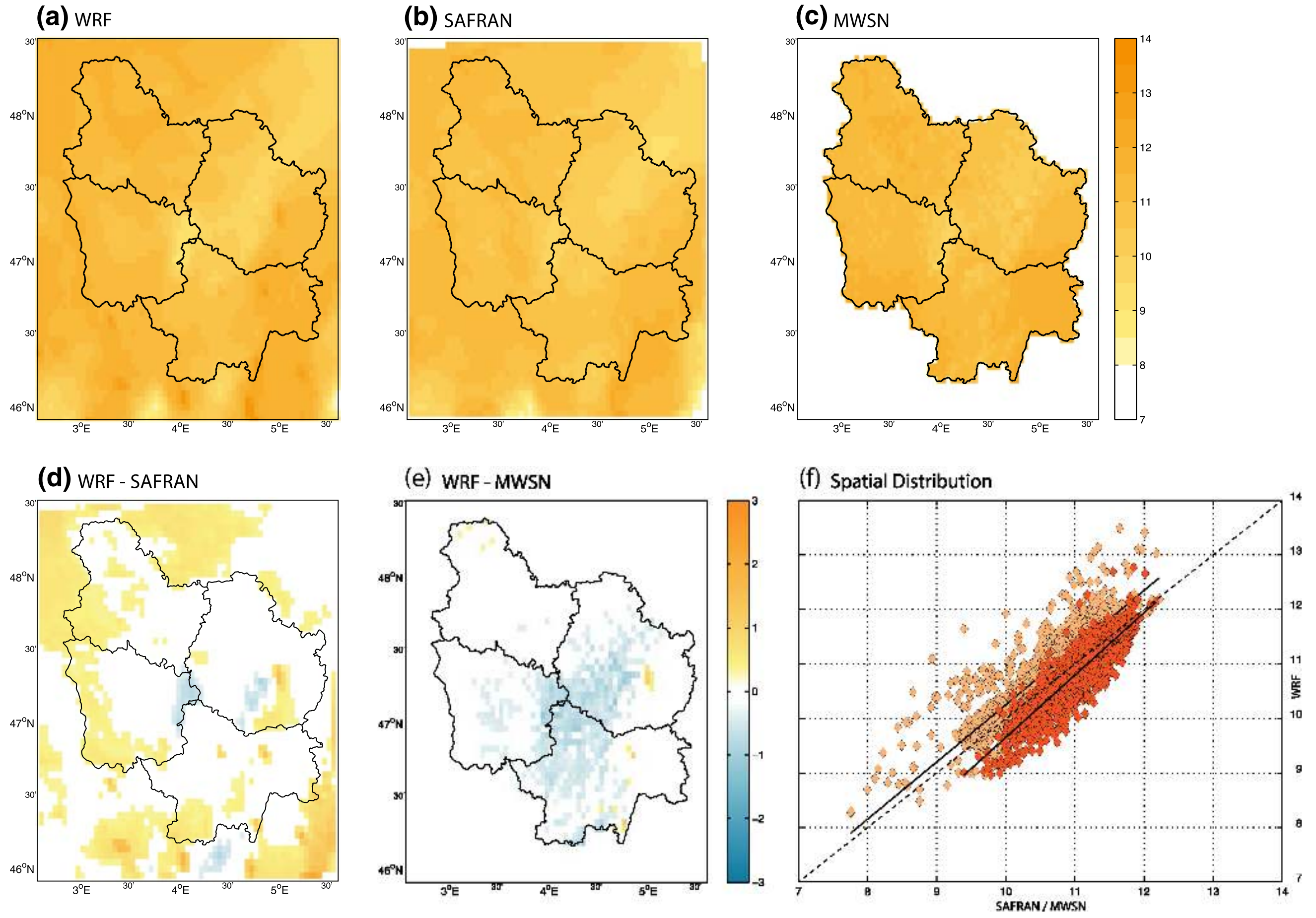

Fig. 2 **a** Annual mean 2 m-temperature (°C) climatology over the period 1989–2008 according to WRF. **b** As (**a**) but for SAFRAN. **c** As (**a**) but for MWSN interpolated records. **d** WRF biases against SAFRAN, period 1989–2008. **e** As (**d**) but against MWSN records. Only differences that are significant at 95 % according to a *t* test are presented. **f** Scatter-plots of annual mean 2 m-temperature for 1989–2008 at all grid-points of the studied area : WRF versus SAFRAN (*orange*) and WRF versus interpolated MWSN records (*red*). *Black lines* show least-square linear regressions

corresponding biases (Fig. 2d, e). Figure 2f presents the corresponding scatter plots. WRF simulates realistic spatial 2 m-temperature variability (Fig. 2) over Burgundy. As expected, the 20-year mean daily 2 m-temperature spatial distribution presents a strong altitudinal gradient with minimum values found over high ground areas (Morvan and seuil de Bourgogne plateau, see Fig. 1b) and maximum values over the northwestern and eastern plains. These results are in good agreement with Castel et al. (2010) and Xu et al. (2012). WRF presents however a cold bias against MWSN records (−0.24 °C for the regional average), mostly located over the central part of the region (Fig. 2e) and over high ground areas. This cold bias is partly generated by an under-estimation of maximum temperatures, already present in ERA-Interim forcings (Xu et al. 2012). A better fit is obtained with MWSN observations than SAFRAN analyses, despite the underestimation of the 2 m-temperature (Fig. 2f). With respect to SAFRAN analyses, the regionally averaged temperature difference is positive (0.29 °C) and spatially contrasted over Burgundy. The spatial pattern of the 2 m-temperature differences between WRF and SAFRAN (Table 2a) is strongly correlated with that of relative humidity differences (r = −0.75), and to a lesser extent to the altitude (r = −0.35). Although less extensive than with MWSN observations, a cold bias is found over central areas, confirming the underestimation of WRF mean 2 m-temperature over the Morvan massif. Warm differences are located over surrounding areas. Note that SAFRAN analyses may themselves exhibit small biases introduced by their hourly interpolation, which does not fully reproduce the observed diurnal cycle during the whole year (Quintana-Seguí et al. 2008).

Figure 3 presents the average annual cycle (Fig. 3a), year-to-year fluctuations (Fig. 3b) of a regional mean

Table 2 (a) Spatial correlations of the differences between WRF and SAFRAN weather variables and altitude over the period 1989–2008 (n = 3886). (b) Temporal correlations (1989–2008, n = 20) of the differences between WRF and SAFRAN weather variables, averaged over the whole region

(a)	Temperature	Relative Humidity	Wind Speed	Solar Radiation	Precipitation
Temperature		-0.75	0.01	0.28	0.11
Relative Humidity	-0.75		0.14	-0.31	0.00
Wind Speed	0.01	0.14		-0.22	−0.19
Solar Radiation	0.28	-0.31	-0.22		0.08
Precipitation	0.11	0.00	-0.19	0.08	
Altitude	-0.35	0.62	-0.04	0.05	0.35

(b)	Temperature	Relative Humidity	Wind Speed	Solar Radiation	Precipitation
Temperature		-0.61	-0.13	0.39	-0.06
Relative Humidity	-0.61		-0.19	-0.49	0.33
Wind Speed	-0.13	-0.19		0.32	0.38
Solar Radiation	0.39	-0.49	0.32		-0.12
Precipitation	-0.06	0.33	0.38	-0.12	

temperature index and the spatial pattern of temporal correlations between WRF and SAFRAN (Fig. 3c) and MWSN (Fig. 3d) annual means. The annual cycle of observed mean temperature (Fig. 3a) is particularly well reproduced by WRF (r = 0.99 with both MWSN and SAFRAN) with a maximum cold bias found during March and April for the both data sets (Table 1). WRF simulation is in better agreement with observed data than the SAFRAN analyses during fall. The warm difference between WRF and SAFRAN is systematically found for every year of the period 1989–2008 (Fig. 3b). It is strongly correlated (Table 2b) with the relative humidity difference between SAFRAN and WRF (r = −0.61) and to a lesser extent the solar radiation difference (r = 0.39). The regional mean 2 m-temperature index shows that, in most years, WRF is closer to the observations than SAFRAN. The interannual variability is also well simulated (r = 0.88 with both MWSN and SAFRAN). From one year to another, WRF best fits observations over the northwestern part of the region (Fig. 3d), and presents minimum correlations over the southeastern part. This gradient is also found in the comparison between WRF and SAFRAN (Fig. 3c). WRF seems to better reproduce 2 m-temperature over areas controlled by westerly frontal disturbances and probably experiences more difficulties to reproduce thermal inversions associated with low-level phenomena during winter over the southeastern areas. These results confirm the model's capabilities to regionalize 2 m-temperature over the region.

3.2 Relative humidity

Only 36 MWSN stations record relative humidity daily (Fig. 1b). Their relative scarcity and heterogeneous distribution forced us to make comparisons with the nearest WRF grid-point. However, grid-to-grid comparison is performed between WRF simulation and SAFRAN analyses.

Relative humidity is related to air temperature as showed in Table 2a, b. Its variation is reversed from that of temperature, as the relative humidity depends upon the saturated vapour pressure, which increases as temperature rises. As expected, Fig. 4 shows that WRF relative humidity is related to the air temperature distribution (Fig. 2), with the highest values mostly located over areas with altitude exceeding 300 m. In sharp contrast, no clear altitudinal gradient appears for MWSN stations. The driest (wettest) stations are mostly located over the lowland (high ground) areas, but observations are strongly affected by local conditions. SAFRAN relative humidity shows a homogenous spatial distribution over the whole region that appears uncorrelated with neither the relief nor the MWSN records. Compared to MWSN, WRF tends thus to produce small dry (wet) biases mostly over the plains (elevated regions) (Fig. 4c). Maximum biases are located close to the major cities (Macon, Dijon, Auxerre, Sens), and are related to the simulation of urban heat islands by WRF (see Fig. 2a). Differences between WRF and SAFRAN show quite a similar spatial distribution. The matrix of spatial correlation (Table 2a) shows that relative humidity differences between WRF and SAFRAN are strongly correlated with the 2 m-temperature differences (r = −0.75), the altitude (r = 0.62) and also the solar radiation (r = −0.31), since the latter is involved in the 2 m-temperature spatial variability. Most of wet differences are located over the Morvan massif in the central parts of Burgundy (>+4 %), which experiences the maximal cold differences for 2 m-temperature, and dry differences predominate over the surrounding plains (<−2 %).

The annual cycle of observed mean relative humidity (Fig. 5a) shows that WRF (1) produces a wet bias during spring; (2) reduces the ERA-Interim dry bias in summer; (3) enhances it in fall, which presents maximum biases and RMSE against MWSN observations (Table 1). ERA-Interim and MWSN observations show very high co-variability (r = 0.98 over 1989–2008), probably due

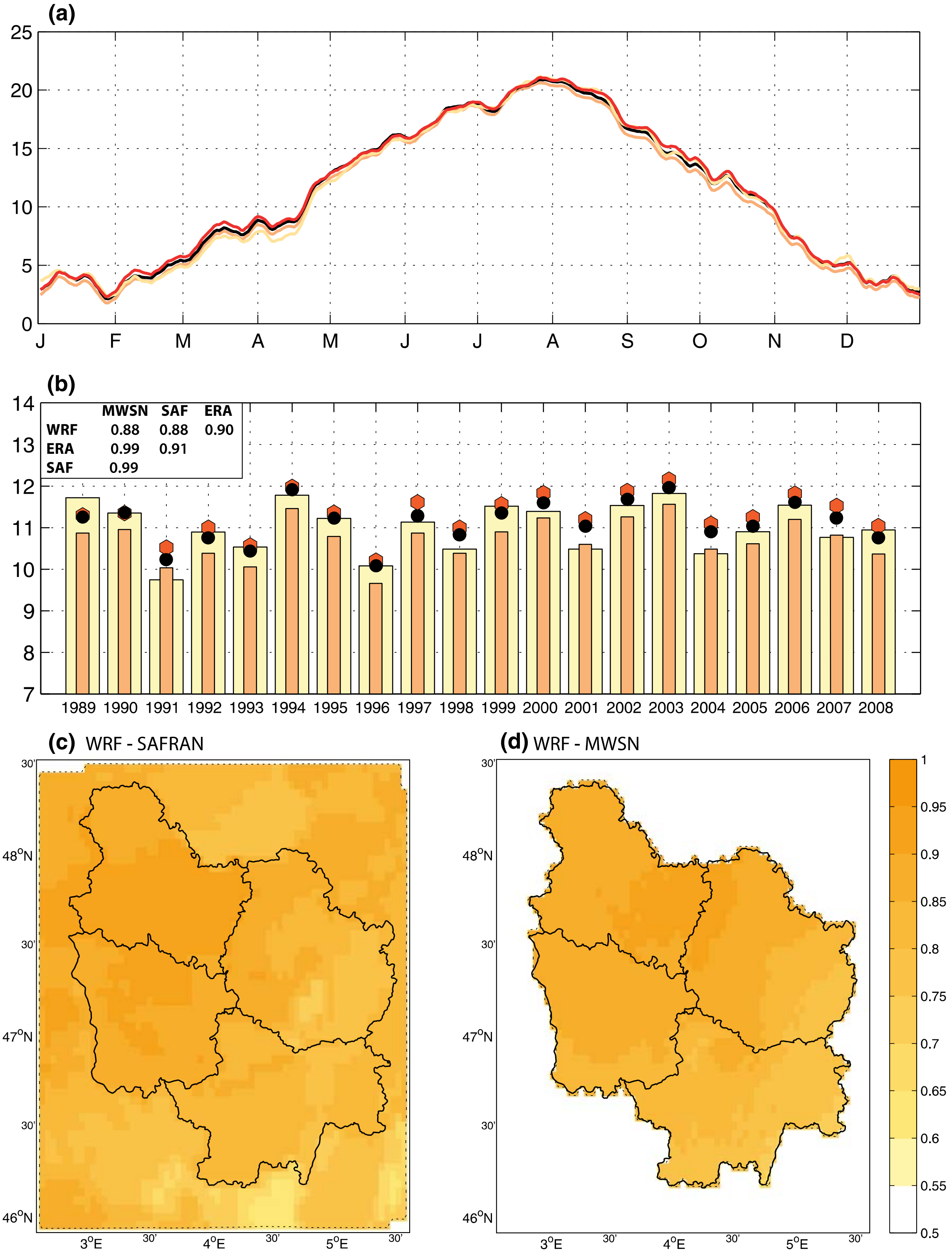

Fig. 3 **a** 2 m-temperature daily mean annual cycle (°C), averaged spatially over Burgundy for WRF exp. (*yellow curve*), SAFRAN analyses (*orange curve*), MWSN records (*red curve*), and ERA-Interim reanalyses (*black curve*), period 1989–2008. **b** As (**a**) but for the **i**nterannual 2 m-temperature index averaged throughout the year. *Colors* are the same as panel (**a**). **c** Correlation between annual 2 m-temperature simulated by WRF and SAFRAN analyses, period 1989–2008. **d** As (**c**) but for WRF and MWSN interpolated records. *Dashed black curves* enclose correlations significant at $P = 0.95$ according to a Bravais–Pearson test

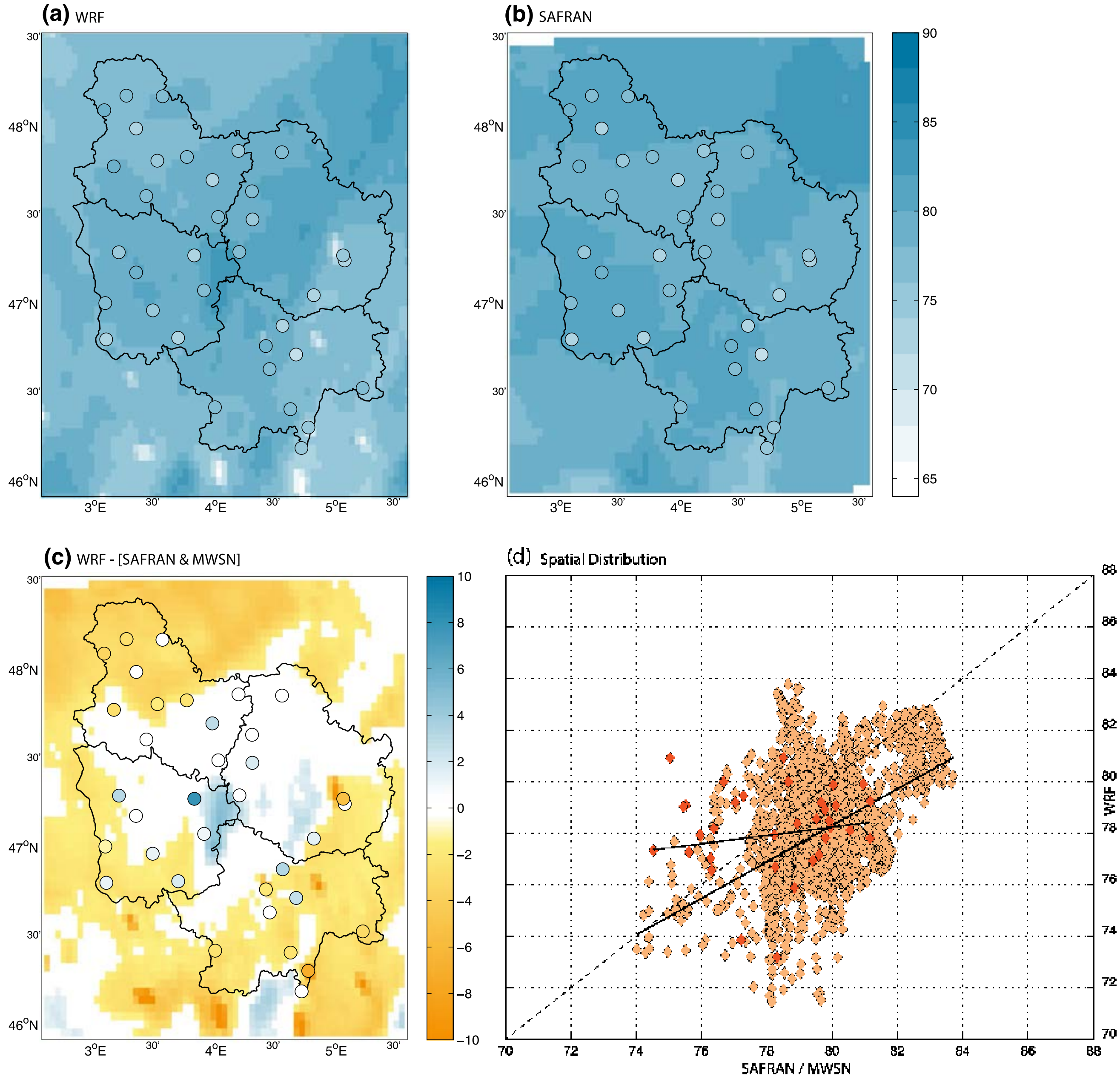

Fig. 4 As Fig. 2 but for annual mean 2 m-relative humidity (%)

to the fact that ERA-Interim data assimilate observation from MWSN records. Even if the relative humidity simulated by WRF exhibits weaker co-variability with MWSN observations (r = 0.84), the dry bias is generally reduced (Fig. 5a). In some months, especially from March to June, WRF actually over-corrects ERA-Interim, which presents an underestimation of up to −10 %, as already stated by Szczypta et al. (2011). Due to the better simulation of the relative humidity over the surrounding plains and cities, the annual mean relative humidity simulated by WRF also better fits the observations for more years than SAFRAN analyses do (Fig. 5b). Temporal correlation matrix (Table 2b) shows that the difference between WRF and SAFRAN is strongly correlated with the 2 m-temperature difference (r = −0.61), but also the solar radiation (r = −0.49). Interannual correlations (Fig. 5c) show that WRF is in fair agreement with SAFRAN ($0.5 \leq r \leq 0.9$) over almost the whole region except the northern part of

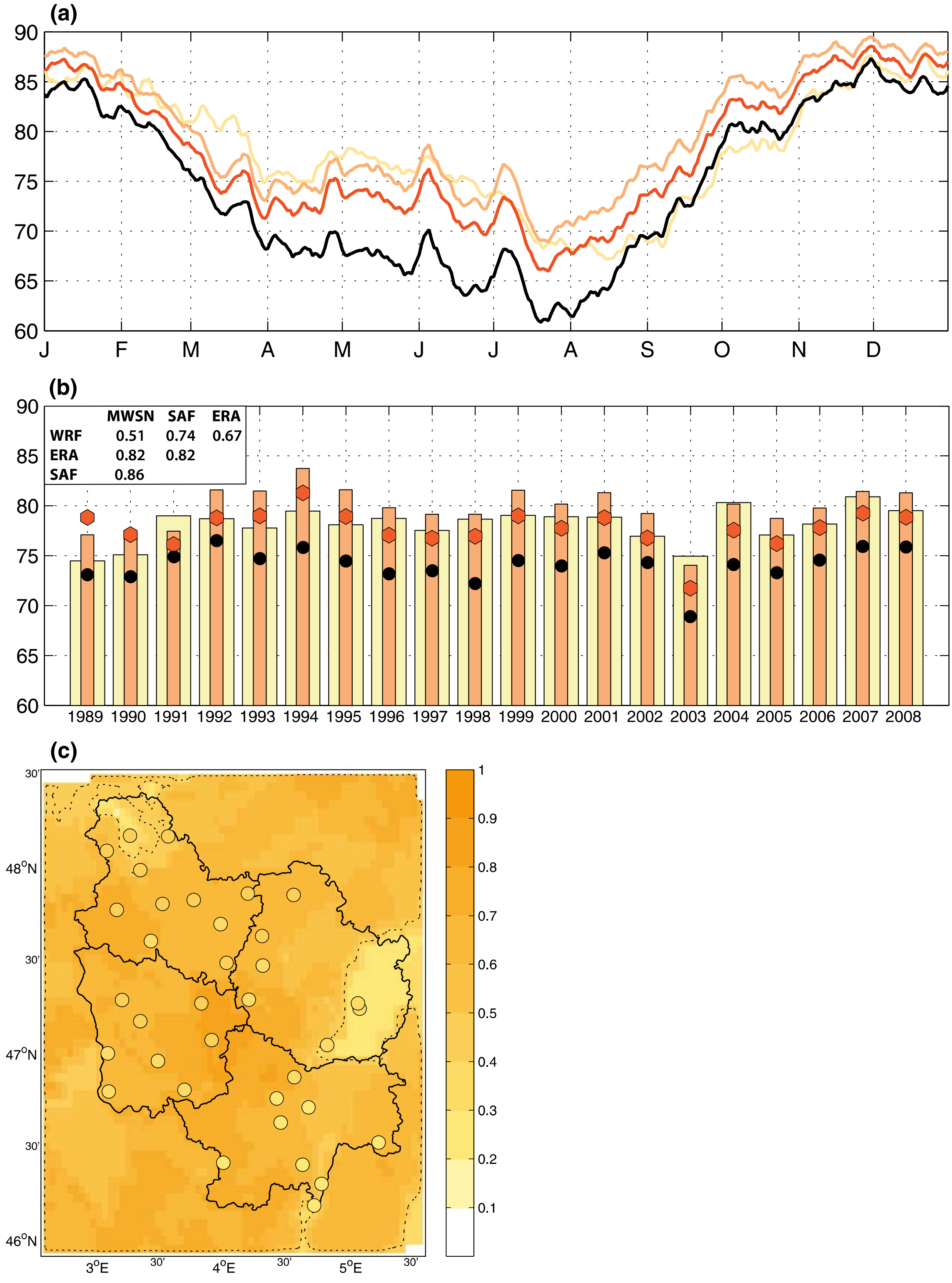

Fig. 5 As Fig. 3 but for 2 m-relative humidity (%)

the Saone Valley and the northwestern part where they are not significant. Temporal correlations between WRF and local MWSN observations show a NW–SE gradient with maximum correlations reaching 0.58 in northwestern Burgundy but becoming not significant over the southeastern part.

3.3 Wind speed

Only 28 MWSN stations are available for wind speed (Fig. 1b), but they present a homogeneous distribution over the region, even if they are mostly located in lowland areas. As for relative humidity, comparison is done with the nearest WRF grid-point but grid-to-grid comparisons are feasible for SAFRAN.

Highest wind speeds simulated by WRF (Fig. 6a) are mostly located in the northern part of Burgundy, where the average wind speed is often higher than 3 m/s. The relationship with topography is unclear, although minimum wind speeds tend to be found in small inner basins. The southern part of the region experiences lower wind speeds (<2 m/s). MWSN observations do not present such clear zonal distribution but also tend to exhibit their highest wind speeds (>2 m/s) over the northern part of the region, and their lowest (<2 m/s) wind speeds over some locations in the southern part of Burgundy. Even if wind speed is highly variable in space within scale of hundreds of meters (Vidal et al. 2010), WRF tends to present an overall positive bias that reaches 1.5 m/s (Fig. 6d) over northwestern Burgundy (Fig. 6c). This overestimation may be attributable to the use of the Yonsei University planetary boundary layer, which has an impact—underestimation of the vertical wind shear—on the wind speed during stable conditions,

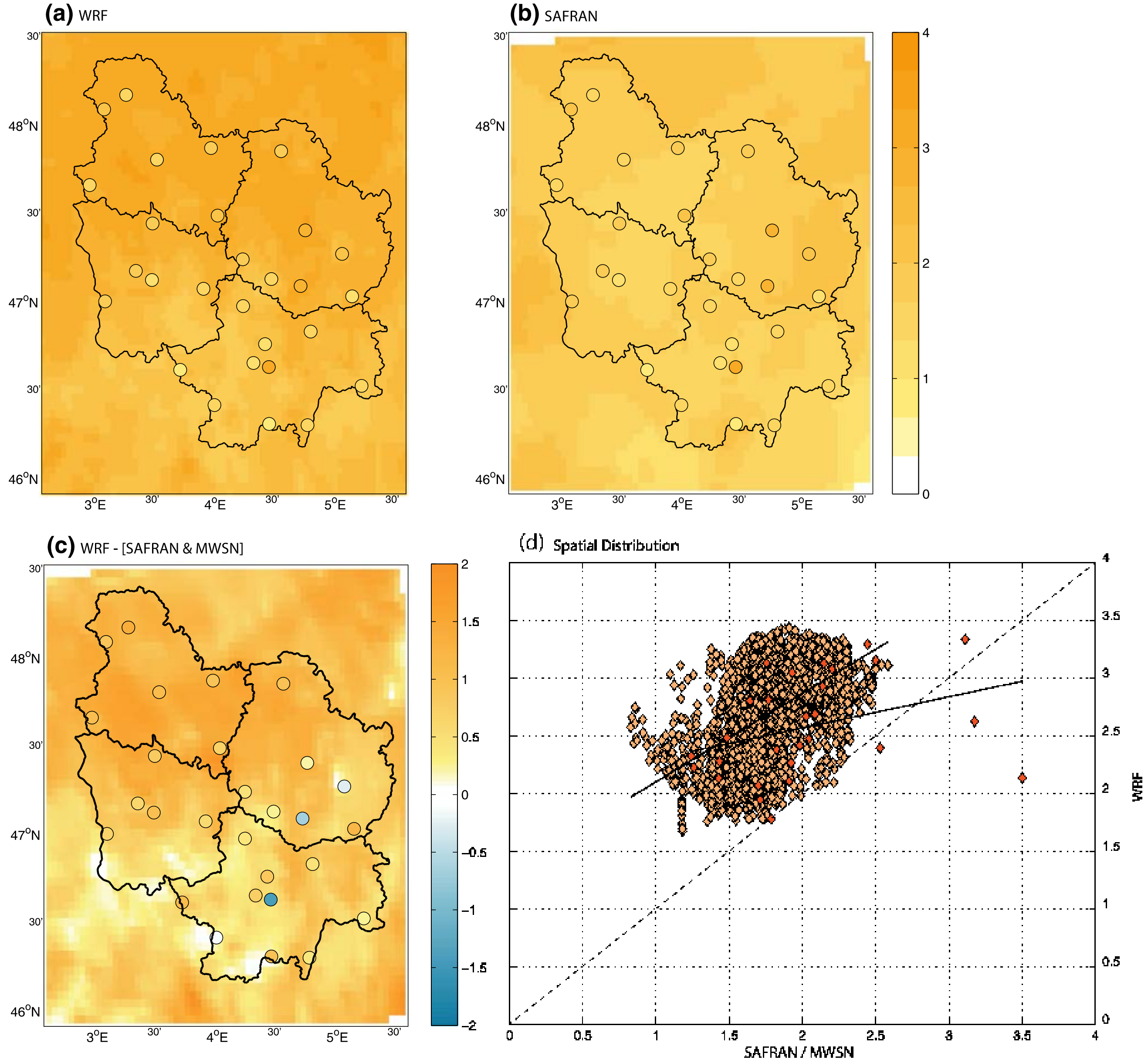

Fig. 6 As Fig. 2 but for annual mean 2 m-wind speed (m/s)

especially during winter. A large wind speed under-estimation (>−2 m/s) is located over an isolated hill, Mont-Saint-Vincent (601 m, central southern Burgundy) and can be attributed to the specific local topography. Indeed, this negative bias is not found over adjacent stations (located in partly urbanized plains), suggesting that WRF smoothes out the wind speed spatial variability. SAFRAN show difficulties to reproduce the spatial distribution (Fig. 6b). The mean wind speed and its spatial variability are under-estimated (Fig. 6c). This result is consistent with Quintana-Seguí et al. (2008) and Szczypta et al. (2011) who concluded that SAFRAN analyses underestimated average wind speed with a mean bias of −0.3 m/s. This bias arises from the hourly interpolation and a spatial linear interpolation, which cannot resolve some local phenomena (Quintana-Seguí et al. 2008). Moreover, Vidal et al. (2010) indicate that the lower accuracy for spatial patterns of wind speed is mainly due to the scarcity of ground-based observations.

The wind speed annual cycle (Fig. 7a) brings similar conclusions. WRF systematically produces higher than expected spatial mean wind speed throughout the year. This positive bias slightly increases from October to February (Table 1). According to Szczypta et al. (2011), this over-estimation is mostly generated by an over-estimation of wind speed transmitted to WRF by ERA-Interim, and is not mitigated by WRF's better resolution, partly due to the use of the Yonsei University planetary boundary layer. At the interannual time-scale (Fig. 7b), both ERA-Interim and WRF, which are highly correlated ($r = 0.72$), present a weak co-variability with SAFRAN ($r = 0.39$ and $r = 0.29$ respectively) and MWSN ($r = 0.53$ and $r = 0.45$), but it should be noted that the actual range of wind speed variations is small. From one year to another, ERA-Interim and WRF's (SAFRAN's) positive (negative) biases appear to be almost constant over the period. Interannual correlations (Fig. 7c) show that WRF presents significant moderate correlations with MSWN observations for 23 of the 28 stations ($r > 0.43$). Only few areas show significant correlations between WRF and SAFRAN. The influence of local processes and the scarce network of observation data, particularly over elevated areas, make it difficult to evaluate the reliability of the three model products (SAFRAN, ERA-Interim and WRF) used in this work.

3.4 Solar radiation

ET_0 estimation is strongly constrained by the reliability of solar radiation data (Bois 2007). Solar radiation is also the main forcing variable that controls ET_0 during the summer season. The small number of in situ solar radiation records is a challenge for modelling ET_0 for climate impact studies (Remesan et al. 2008). In order to estimate the reliability of solar radiation simulated by WRF, only 9 MWSN stations are available (Fig. 1b), which are compared to the nearest WRF grid point. We also perform grid-to-grid comparisons between SATMOS, SAFRAN and WRF. SATMOS data were evaluated over the whole France by Piedallu et al. (2007). They exhibit high skill to reproduce solar radiation, in spite of a positive bias against the 42 MWSN stations between March and July, especially over mountainous areas.

WRF (Fig. 8a) seems to simulate a realistic solar radiation latitudinal gradient, with lower values over the northern part and higher values over the southern parts of the region, consistent with the SATMOS estimates (Fig. 8c) and to some extent with the few MWSN stations available over Burgundy. In contrast, SAFRAN analyses do not show any latitudinal gradient (Fig. 8b). Their highest values are located over the Morvan Massif (>1300 J/cm^2), which is irrelevant considering the expected climatological pattern of a high local cloudiness. Observed radiation is not assimilated in SAFRAN, so a patchy pattern is generated by the optimal interpolation applied over the climatically homogeneous areas. Differences in the spatial distribution between WRF and SAFRAN (Fig. 8d) follow the same pattern, with negative differences over the Morvan Massif, and mainly positive differences over the surrounding plains. WRF simulates lower solar radiation than SATMOS, especially over the southern part of Burgundy (Fig. 8e), but the bias generally remains of moderate magnitude (Fig. 8f). Comparisons with MWSN denote a rather good agreement with the observations, albeit moderate over-estimation (<100 J/cm^2) in some stations in the plains. This could be due to WRF missing cases of local radiative fog in the valleys.

All the solar radiation datasets present a similar annual cycle. At wintertime, when the solar radiation is low, differences between all datasets are negligible (Fig. 9a). Seasonality in the biases is discernible with an over-estimation of solar radiation around 250 J/cm^2 (Table 1) in June-July. A lower positive bias is also found in ERA-Interim and SATMOS data over the whole year. In contrast, SAFRAN shows weak differences in regards to MWSN throughout the year. As shown by Szczypta et al. (2011), ERA-Interim tends to over-estimate the solar radiation, which is consistent with the underestimation of precipitation (Sect. 4.1), while SAFRAN tends to underestimate the solar radiation. WRF improves upon the raw ERA-Interim data, which present a positive bias close to 6 %, and reduces it to a positive bias close to 3 %, but it shows a larger overestimation starting at end of spring and during summer. This overestimation occurring during the core of the convective season is mainly due to the fact that in WRF the subgrid-scale convective parameterization does not consider cumulus cloud feedbacks to radiation. Hence when summertime convection is predominant,

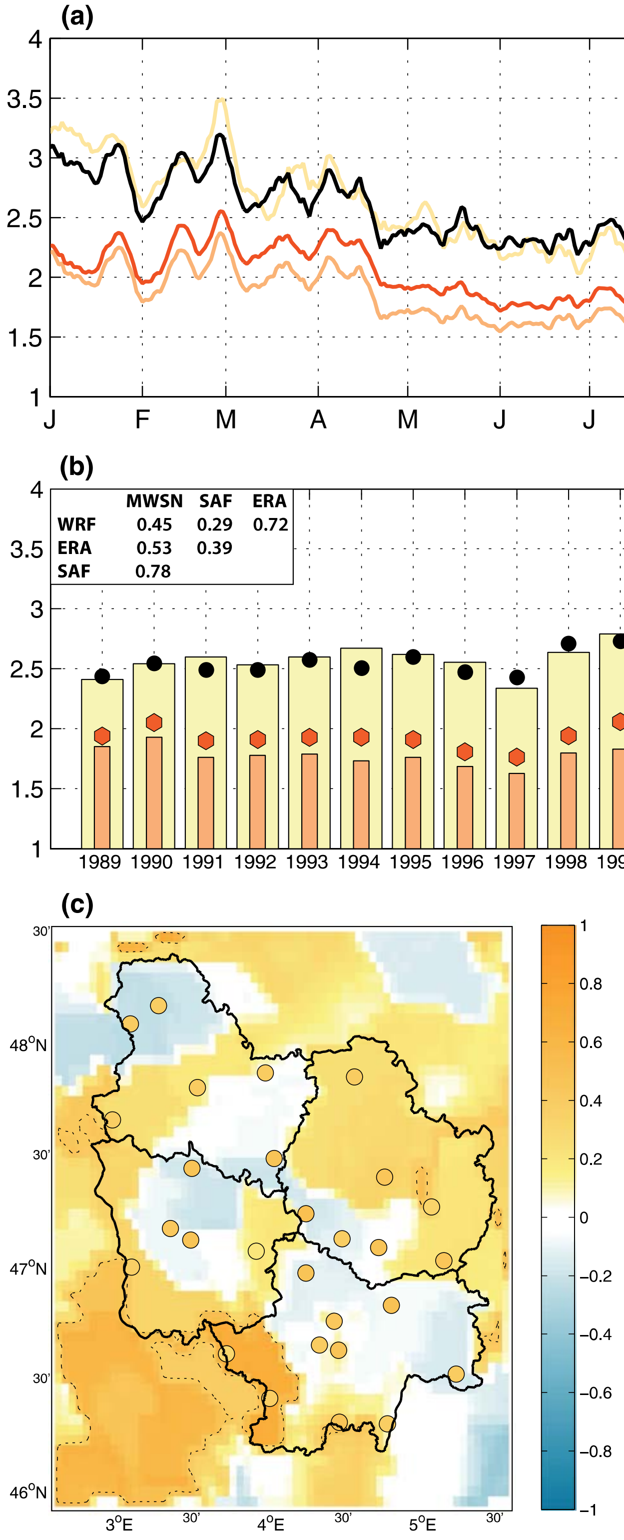

	MWSN	SAF	ERA
WRF	0.45	0.29	0.72
ERA	0.53	0.39	
SAF	0.78		

Fig. 7 As Fig. 3 but for 2 m-wind speed (m/s)

radiatively passive cumulus clouds result in excessive surface radiant energy (Alapaty et al. 2012). One strong limitation of these analyses is however that only three stations are located South of 47°N. The scarcity and the anisotropic distribution of MWSN observations questions the representativeness of a regional solar radiation index, and

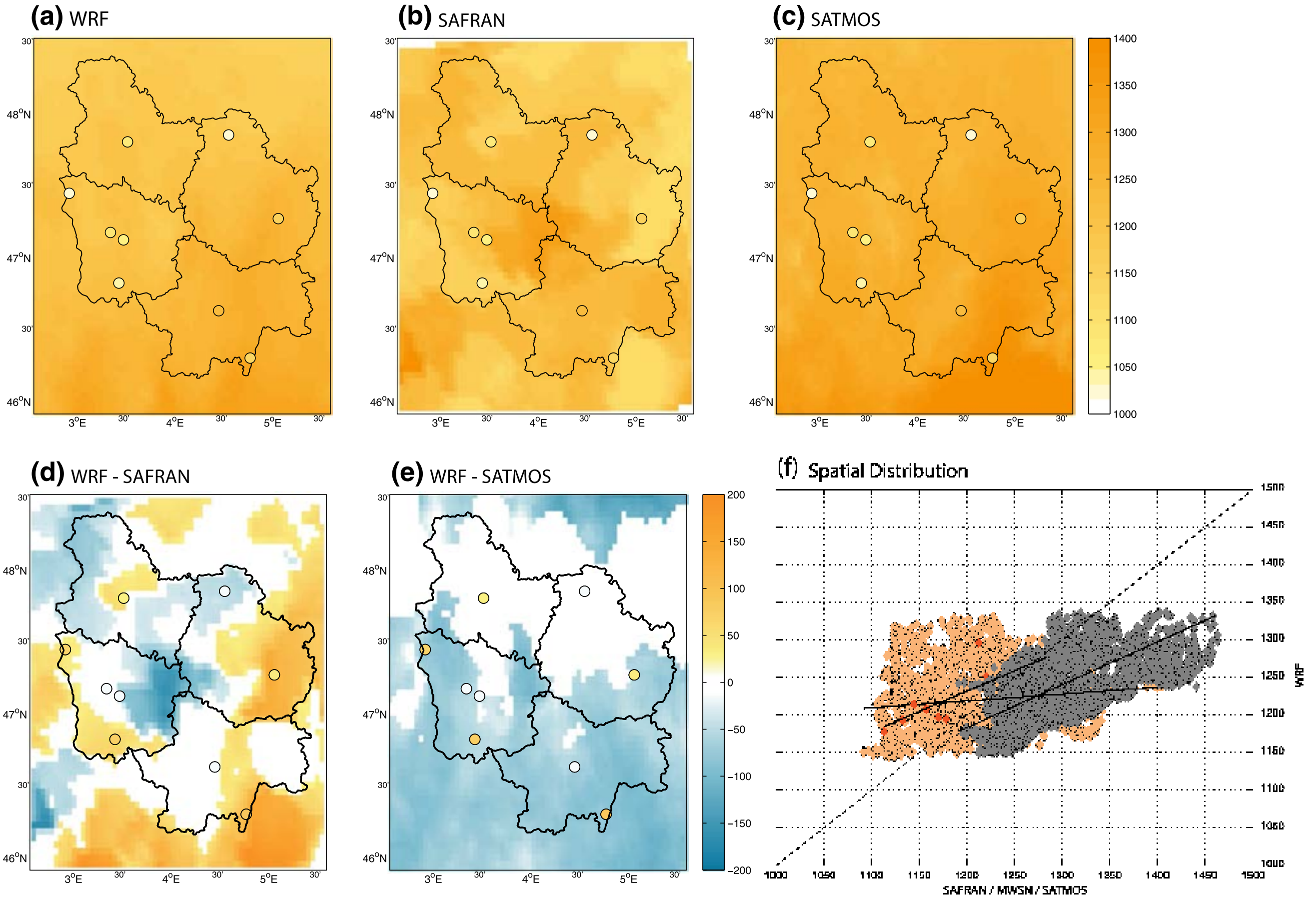

Fig. 8 **a** Annual mean solar radiation (J/cm^2) climatology over the period 1989–2008 according to WRF. **b** As (**a**) but for SAFRAN. **c** As (**a**) but for SATMOS. *Circles* correspond to MWSN station records **d** WRF biases against SAFRAN, period 1989–2008. **e** As (**d**) but against SATMOS. Only differences that are significant at 95 % according to a *t* test are presented. **f** Intercomparison of WRF exp. over the studied area through scatter-plots of annual solar radiation for 1989–2008: WRF versus SAFRAN (*orange*), WRF versus SATMOS (*grey*) and WRF versus MWSN station records (*red*)

can generate an underestimation of the real annual cycle. The interannual variability simulated by SAFRAN and estimated by SATMOS (Fig. 9b) are strongly correlated to MWSN (r = 0.86 and 0.87, respectively). WRF and ERA-Interim are both strongly correlated with SATMOS data (r = 0.78) but WRF shows a lower covariability with MWSN (0.63). WRF reduces the positive bias between ERA-Interim and MWSN observations every year of the period, but the magnitude of their differences varies interannually. Similarly to the results presented in Fig. 7c, the spatial distribution of interannual correlations between WRF and SAFRAN is strongly influenced by the climatically homogeneous areas used in these analyses (Fig. 9c). However, WRF shows high correlation with SATMOS data over the whole region (Fig. 9d). Correlations between WRF and MWSN are weaker but significant, with values ranging from r = 0.43 in the southern part of the region, to r = 0.58 over the northern part. SAFRAN fails at reproducing solar radiation, which is a key variable for the ET$_0$ estimates.

Section 3 illustrated the capability of the WRF model in simulating climate variability over Burgundy at annual and interannual timescales for the atmospheric variables used to compute ET$_0$. The WRF model tends to partially reduce the ERA-Interim biases against MWSN during the vegetative period for 2 m-temperature, relative humidity and wind speed, but slightly degrades the seasonal and interannual variability. Results show a good skill of the WRF model to simulate the spatial distribution for 2 m-temperature and wind speed, relative humidity and solar radiation. However it tends to slightly over-estimate wind speed during winter and solar radiation during summer. At a similar resolution, the spatial distribution for relative humidity, wind speed and solar radiation seems to be more relevant considering the physiography and land-cover of the area than that derived from SAFRAN analyses.

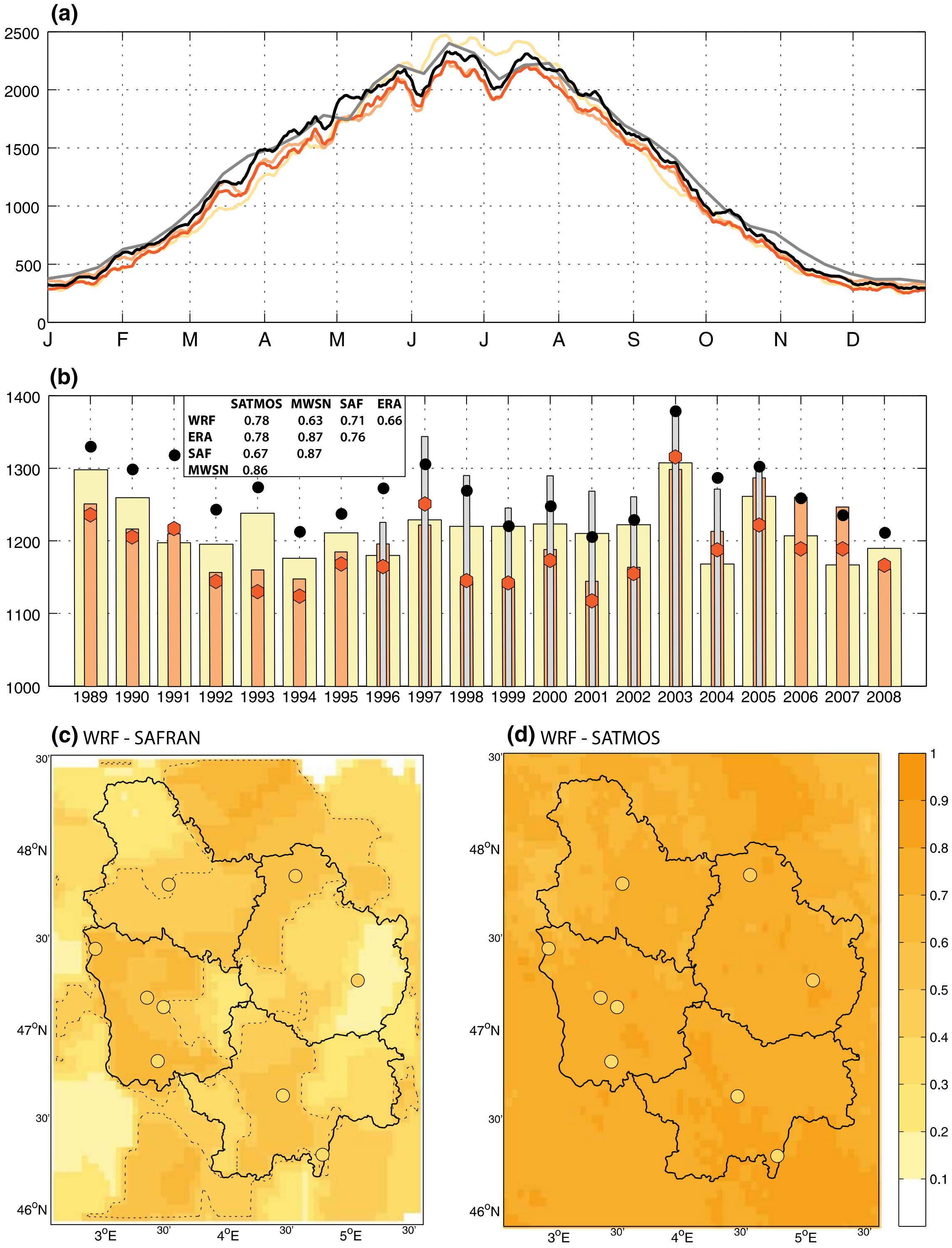

	SATMOS	MWSN	SAF	ERA
WRF	0.78	0.63	0.71	0.66
ERA	0.78	0.87	0.76	
SAF	0.67	0.87		
MWSN	0.86			

Fig. 9 **a** Solar radiation daily mean annual cycle (J/cm^2), averaged spatially over Burgundy for WRF exp. (*yellow curve*), SAFRAN analyses (*orange curve*), MWSN station records (*red curve*), SATMOS satellite data (*grey curve*) and ERA-Interim reanalyses (*black curve*), over the period 1989–2008. **b** As (**a**) but for the interannual solar radiation index averaged throughout the year. *Colors* are the same as panel (**a**). **c** Correlation between annual 2 m-temperature simulated by WRF and SAFRAN, period 1989–2008. **d** As (**c**) but for WRF and SATMOS. *Circles* represent the correlation between WRF and MWSN. *Dashed black curves* correspond to 95 % significant correlations according to a Bravais–Pearson test

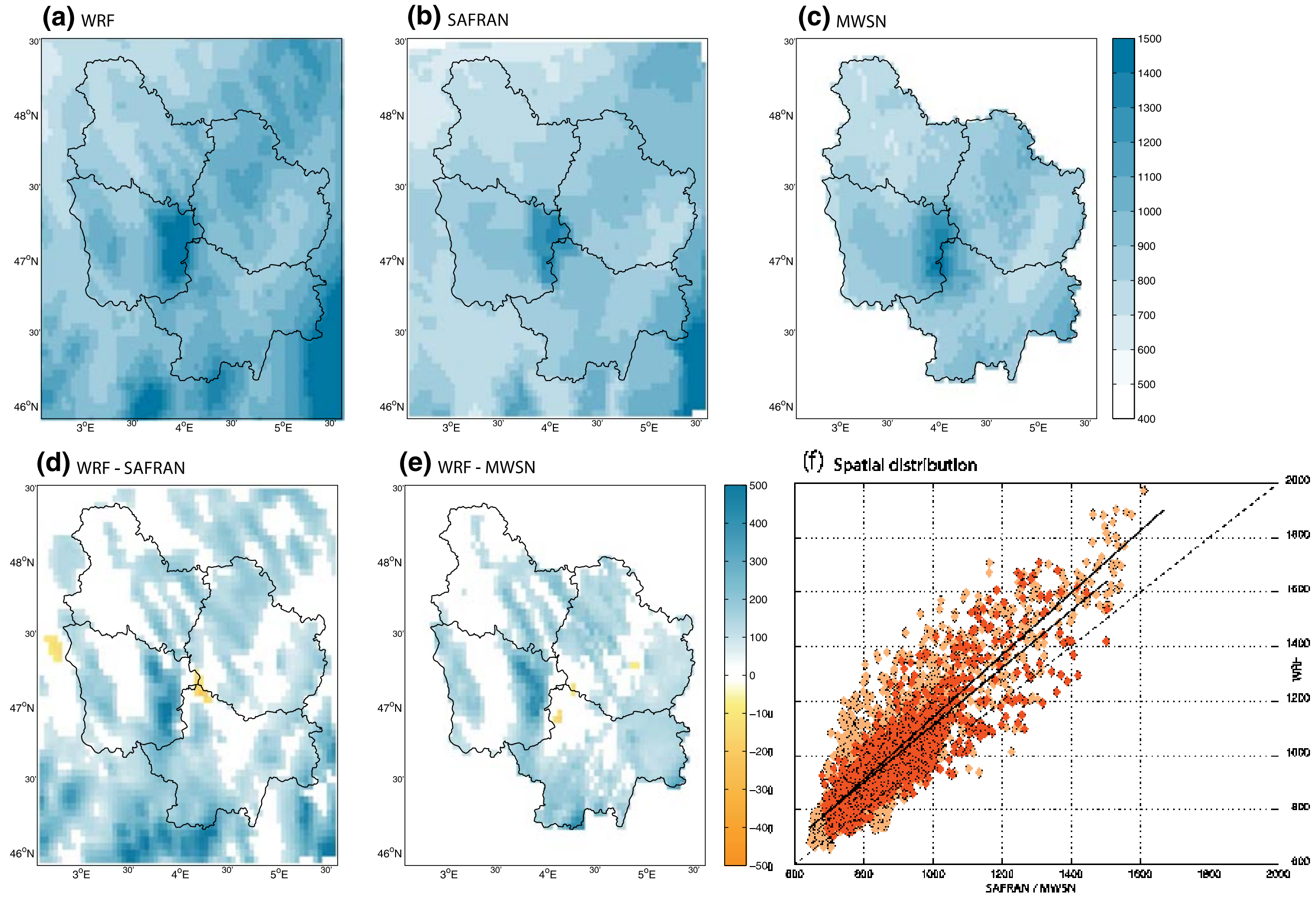

Fig. 10 As Fig. 2 but for annual mean precipitation amounts (mm)

4 Analysis of water balance and its components

This section first presents the results obtained for downscaled precipitation and the reference ET_0 estimated from the Penman–Monteith equation (Allen et al. 1998). The ET_0 computation uses downscaled 2 m temperature, relative humidity, wind speed and solar radiation discussed in Sect. 3. The aim of this section is to evaluate the capability of the model to produce realistic input data (precipitation and ET_0) to compute the soil water balance of Douglas-fir forested stands.

4.1 Precipitation

A detailed study of WRF capability to simulate precipitation over Burgundy is provided in Marteau et al. (2014). Only a brief account is provided here, with SAFRAN and MWSN used as reference datasets, the latter being interpolated onto a 1 km resolution grid using the thin plate splines method. WRF simulates rather realistic precipitation spatial distribution and amounts (Fig. 10a), corroborating the sensitivity studies performed by Castel et al. (2010) and Marteau et al. (2014) over a similar domain. Largest amounts are located over the western slopes of the Morvan Massif (>1500 mm), and minimum amounts over the surrounding plains (<700 mm). This is supported by MWSN (Fig. 10c) and SAFRAN (Fig. 10b). However, precipitation amounts tend to be over-estimated over most parts of the region. Precipitation biases (Fig. 10d, e) are generally moderate, with some noticeable too wet conditions over the relief (>400 m), especially over the southwest side located under the direct influence of the dominant winds. Precipitation amounts simulated by SAFRAN are close to the observations, but underestimate precipitation amounts over the southwest part of the Morvan massif, by about 200 mm (Fig. 10b).

WRF produces less satisfactory results when working on the average annual cycle (Fig. 11a; note that all cycles were filtered using a 31-day running mean for readability). WRF presents a weak co-variability with MWSN observed annual cycle (r = 0.47). The largest differences are found during the spring and summer seasons, from April to August, due to a large over-estimation of convective precipitation (Marteau et al. 2014). This is partly supported by

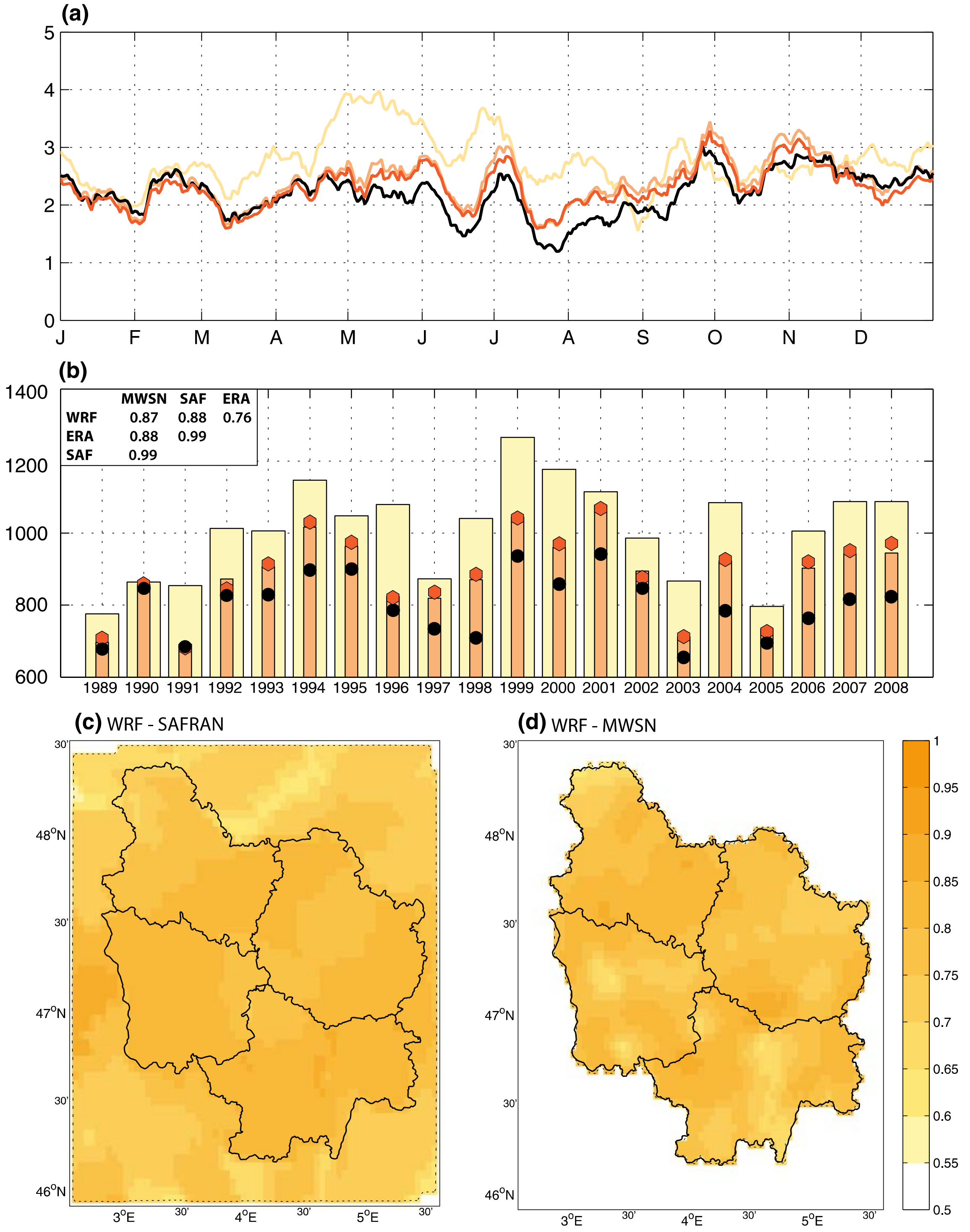

	MWSN	SAF	ERA
WRF	0.87	0.88	0.76
ERA	0.88	0.99	
SAF	0.99		

Fig. 11 As Fig. 3 but for precipitation (mm)

the results of Alapaty et al. (2012) which show over the US that summertime convective systems simulated by WRF model are highly energetic and often lead to a convective instability, resulting in too frequent activations of parameterized convection. Although it over-estimates both the occurrence of rainy days (>1 mm) and their intensity (not shown), WRF shows a better ability to reproduce winter precipitation amounts, mostly controlled by non-convective precipitation, and to a lesser extent fall precipitation amounts, which are slightly underestimated. ERA-Interim reanalyses underestimate precipitation, mainly during the summer season, while SAFRAN is remarkably close to observation.

Figure 11b shows precipitation interannual variability. WRF standard deviation (132.6 mm) is close to those obtained for MWSN (114.4 mm) and SAFRAN (111.5 mm). Simulated annual precipitation also shows a strong co-variability with these datasets (r = 0.87 and 0.88, respectively). As expected, WRF shows a systematic overestimation of the annual precipitation amounts (+122.8 mm against MWSN). The very dry years 1991, 2003 and to a lesser extent 2005 are too wet in the model mostly due to the over-estimation of convective precipitation during spring and summer. The year 1996, an "average" year in Burgundy in terms of annual precipitation amounts, is one of the wettest of the period according to WRF, with an over-estimation of precipitation during winter, spring and summer. WRF downscaling does not affect the performance of the simulated interannual variability (r = 0.88 between ERA-Interim and MSWN) but it over-corrects the underestimation of the annual precipitation amounts found in ERA-Interim (Szczypta et al. 2011). Local interannual correlations (Fig. 11d) show that the model performs rather well (correlations ranging from 0.7 to 0.9) and reproduces accurately the geography of interannual precipitation variability. Spatial correlations (not shown) between WRF and MWSN seasonal fields from one year to another show values that range between 0.64 (in 2006) and 0.86 (in 1995). WRF produces nonetheless less satisfactory results when working on seasonal anomaly fields, i.e. after removal of the climatological precipitation. Spatial correlations are lower and even negative 3 years out of 20, denoting a lower skill for simulating departures from the climatology, and thus climate interannual variability (and associated effects on local precipitation). In contrast, due to the assimilated observation data, SAFRAN is highly correlated to MWSN seasonal anomaly fields with a correlation coefficient ranging from 0.63 in 1993 to 0.90 in 1996.

4.2 Potential evapotranspiration

ET_0 estimates computed from WRF, ERA-Interim and the SAFRAN data are compared with those obtained from the 24 MWSN stations, available for 2004–2008.

Minimum amounts of simulated ET_0 (<700 mm) are found over elevated areas (Fig. 12a), ET_0 increasing as altitude decreases, with slightly larger values over the main cities, presumably due to the simulated urban heat island increasing the temperature locally. This spatial distribution is coherent with the MWSN estimates. SAFRAN is less capable to reproduce this spatial pattern and displays maximum ET_0 amounts over both southeastern Burgundy (as in WRF) and the Morvan massif. Over 2004–2008, with respect to MWSN local stations, WRF underestimates ET_0 amounts over almost the whole region with maximum (minimum) biases located over high ground areas (surrounding plains) (Fig. 12c). This negative bias is not found with SAFRAN: WRF shows higher positive differences over almost the whole region, except the Morvan massif. Due to the uncertainties found in the SAFRAN data for some variables used in the computation of ET_0, it is unsure whether these differences point to deficiencies in WRF, considering the fact that differences of the opposite sign are found with MWSN data. WRF actually presents a lower bias with MWSN (−0.07 mm/day: Table 1) than with SAFRAN (0.23 mm/day), with maximum differences during summer. RMSE are similar in both datasets, at 0.37 mm/day for MWSN and 0.30 mm/day for SAFRAN, which is almost 15 % of the mean ET_0 but still much lower than the values found by Ishak et al. (2010) who reached a 30–40 % error between estimates from observed weather variables and the MM5 model.

All the estimated ET_0 datasets present a similar annual cycle (Fig. 13a). Both of them are highly correlated (r > 0.94) with observations. As expected, almost no bias is found in winter. It is higher during spring and summer, mostly from March to August, probably due to vegetative activity. WRF improves the ERA-Interim ET_0 annual cycle, reducing the strong overestimation mostly due to the solar radiation over-estimation, and a better representation of land surface. In contrast, SAFRAN slightly underestimates ET_0, mostly during the summer season, with a bias reaching 1 mm/day, mostly due to the underestimation of both wind speed and solar radiation. The interannual variability derived from SAFRAN and MWSN are strongly correlated (Fig. 13b). WRF also systematically underestimates ET_0 but seems to produce weaker biases than ERA-Interim. WRF shows a lower covariability with MWSN (r = 0.83) than ERA-Interim (r = 0.96). Temporal correlations (Fig. 13c) show that WRF is in good agreement with MWSN estimates over almost the whole region except for localized stations, all located in the northern part of the region. Temporal correlations between WRF and SAFRAN present more discrepancies, with low correlations over the eastern area, mainly attributable to the poor accuracy of SAFRAN wind speed and solar radiation. The patchiness associated with the SAFRAN product also appears clearly. These results are also verified when working on a potential evapotranspiration calculated with the Penman Formula and computed from the Biljou© model for each Douglas-fir stands (Fig. 14) over the 1989–2008 period. The annual cycle (Fig. 14a) is well reproduced (r = 0.99 between WRF and MWSN). WRF produces less satisfactory results (Fig. 14b) for the interannual variability (r = 0.59), this weaker correlation is partly explained by the distance between some MWSN weather variables to the Douglas-fir stands as the solar radiation data.

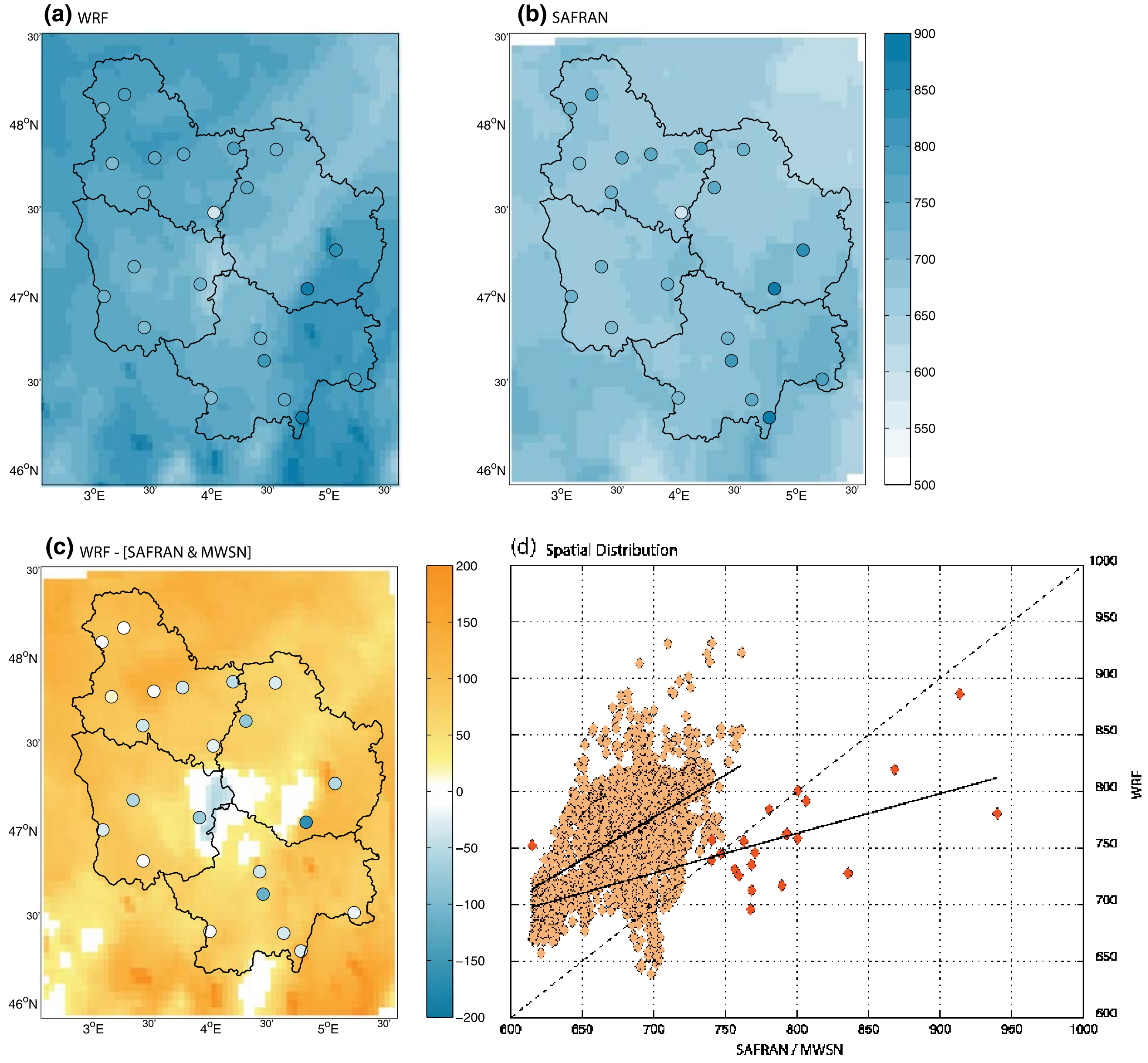

Fig. 12 As Fig. 2 but for annual mean reference evapo-transpiration amounts (mm)

To sum up, the WRF model seems capable to produce ET_0 fields with a reasonable accuracy, suggesting its potential usefulness for impact studies. An illustration is proposed in the next section.

4.3 Computation of the water balance for Douglas-fir stands

To assess the reliability of the WRF model to simulate weather variables involved in the ET_0, a local scale indirect assessment based on the daily soil water balance of 30 Douglas-fir stands, which present a high sensitivity of their radial growth to soil water deficit events, was computed using the process-based model Biljou© (Granier et al. 1999). The MWSN, SAFRAN and WRF weather variables nearest to the 30 Douglas-fir stands (mostly located over central and southern Burgundy, see Fig. 1c) are used as climatic input. Potential evapotranspiration is computed by Biljou© according to the Penman equation prior to the water fluxes modeling.

Differences between the mean soil water deficit index (SWDI) computed with WRF and MWSN records (Fig. 15a) present a heterogeneous distribution with larger differences (ranging from 10 to 27 %) over the eastern part (and especially the northernmost three stands: 31–42 %), while smaller differences (<10 %) prevail for 9 of the 12

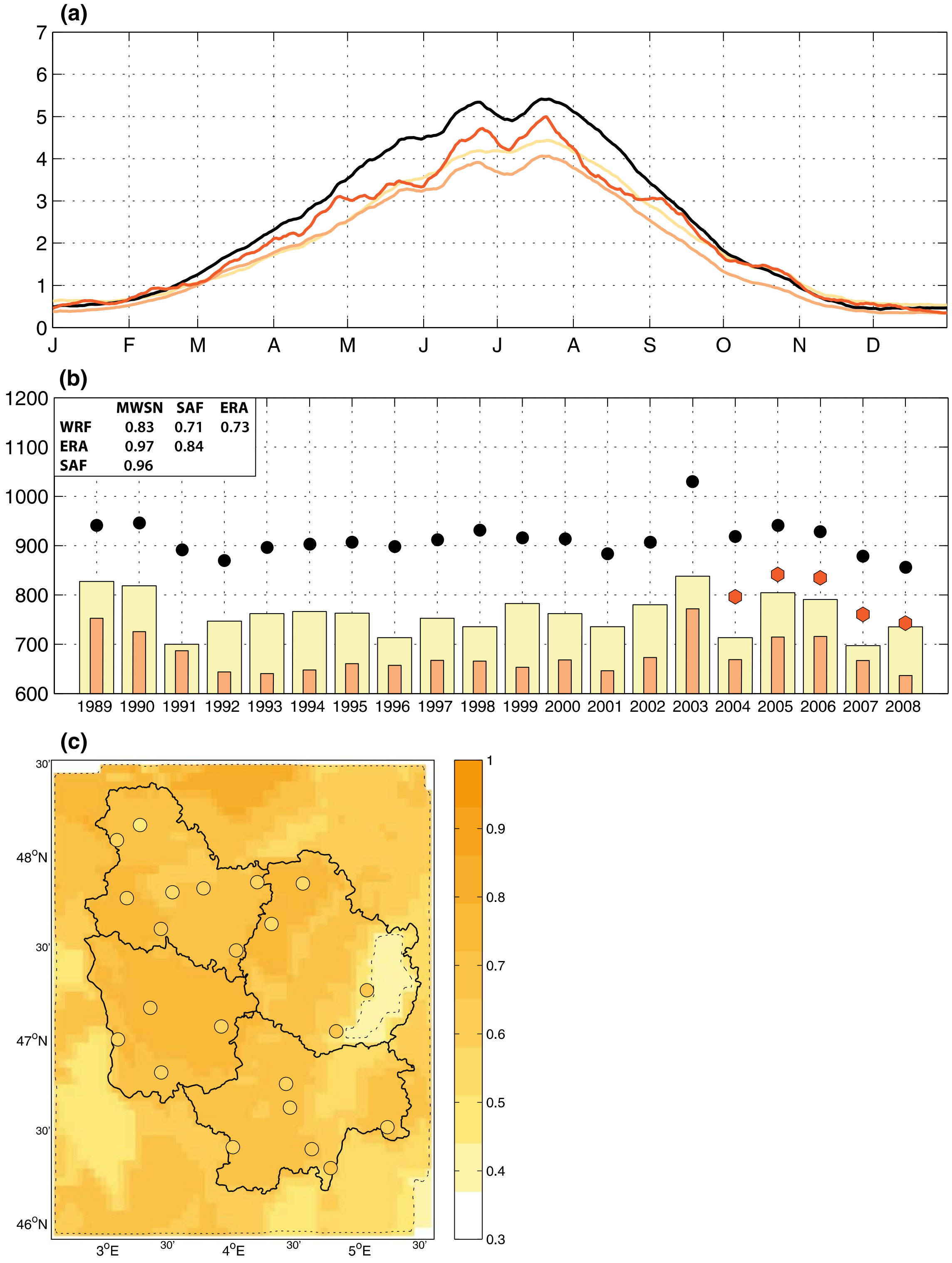

	MWSN	SAF	ERA
WRF	0.83	0.71	0.73
ERA	0.97	0.84	
SAF	0.96		

Fig. 13 As Fig. 3 but for reference evapo-transpiration amounts (mm)

stations located in the western part of the domain. These smaller differences can be attributed to the lower soil water deficits experienced over the windward wetter side of the Morvan massif. Interannual variations of SWDI computed by Biljou© for the 30 Douglas-fir stands and using WRF data and MWSN as climatic input present an average correlation of 0.34 over the period 1989–2008, with large inter-station discrepancies. Higher and significant correlations

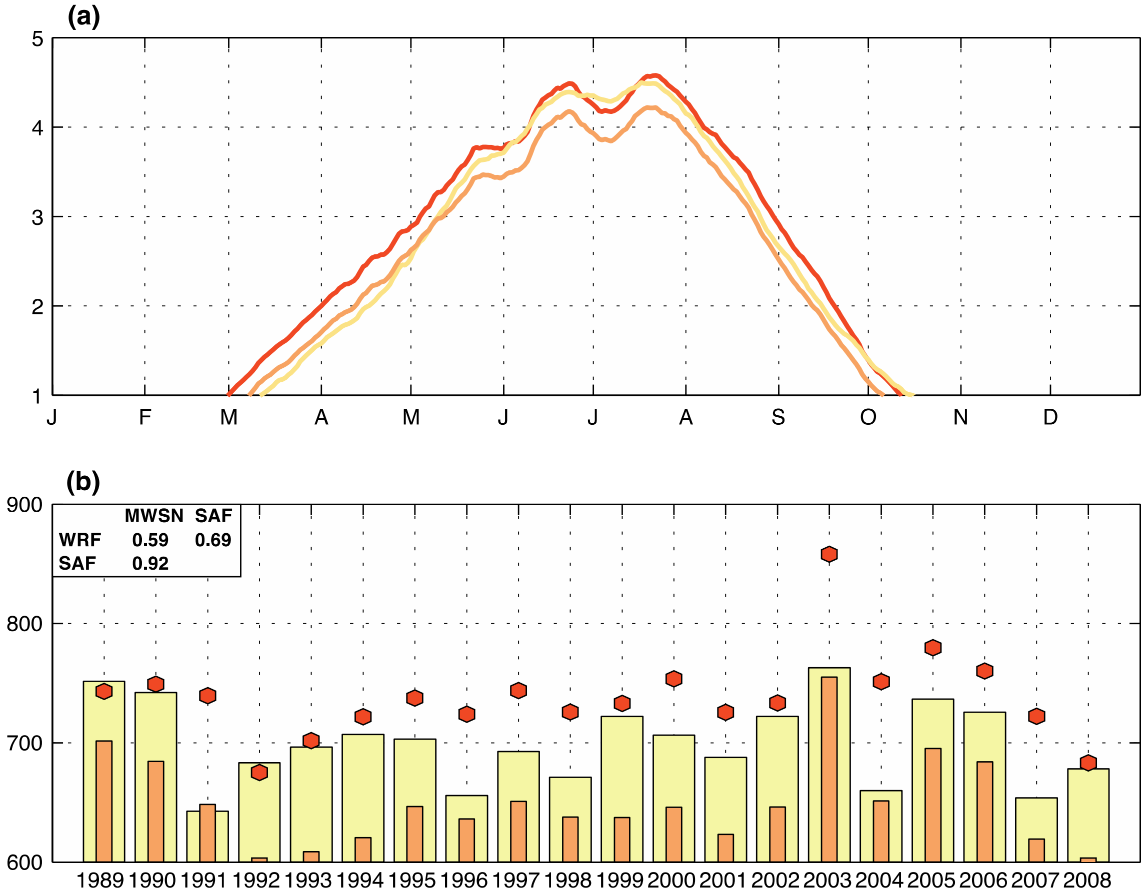

Fig. 14 As Fig. 3 but for Penman evapo-transpiration amounts computed with Biljou© (mm)

are found outside the Morvan massif, whereas they are strongly contrasted over the massif itself. This suggests that the higher spatial variation of climatic parameters over hilly terrain is inadequately sampled by the few weather stations available over this area.

Figure 15b presents the average Relative Extractable Water (REW) computed with the same climatic datasets for the thirty Douglas-fir stands, plus one experiment merging MWSN precipitation and other variables taken from WRF simulations. The REW computed from WRF raw data is highly correlated with that computed from SAFRAN and MWSN ($r = 0.83$). However, WRF overestimates the REW from May to October. This overestimation is a key issue that affects the ability of WRF to produce a consistent SWDI, since SWDI corresponds to the sum of the daily deviations between the relative extractible water and the critical value of 40 %. In July–August average REW is close to this value (Fig. 15b), hence small REW biases may translate into large SWDI biases (Fig. 15c). The REW overestimation is sensibly reduced during spring and close to the MWSN REW during summer (Fig. 15b) when computed from the merged dataset (i.e., when replacing WRF-simulated rainfall by observation). Substituting observed precipitation to WRF simulations also strongly improves the realism of the SWDI ($r = 0.97$ between the SWDI computed from WRF + MWSN precipitation and that computed from MWSN) and presents smaller differences to MWSN SWDI than SAFRAN (Fig. 15c). In order to further assess the contribution of each WRF variable used as input in the soil water balance computation, four other experiments were carried out for the thirty Douglas-fir stands. As for the experiment replacing WRF-simulated rainfall by observation discussed above, the four analyses were performed by substituting one by one each WRF variable by the corresponding MWSN observations (Fig. 15c). Note that the MWSN weather records, especially for solar radiation, are taken from stations located at some distance of the Douglas-fir stands (Fig. 1b), which can explain part of the differences between SWDI computed from WRF and MWSN. Comparisons between these experiments and SWDI computed from MWSN and SAFRAN data reveal that the low capacity to reproduce the soil water content with the WRF model is mainly caused by its large precipitation biases. In contrast, substituting simulated relative

Fig. 15 **a** Differences in percentage *(colors)* and correlations *(circle size)* between SWDI computed with Biljou© using raw WRF data and MWSN records climatic input for the 30 Douglas-fir stands. **b** Mean annual cycle (1989–2008, average of the 30 Douglas-fir stands) of the Relative Extractable Water computed from WRF (*yellow curve*), SAFRAN (*orange curve*), MWSN (*red curve*) and WRF + MWSN precipitation (*black curve*) data. **c** Yearly mean intensity of the SWDI for the 30 Douglas-fir stand computed with MWSN nearest records (*red curve*), SAFRAN *(orange curve),* raw WRF (*yellow curve*), WRF + MWSN precipitation (*black curve*), WRF + MWSN temperature (*dark grey curve*), WRF + MWSN wind speed (*grey curve*), WRF + MWSN relative humidity (*light grey curve*), and WRF + MWSN solar radiation (*lighter grey curve*) data, period 1989–2008. **d** Interannual variations in the growth index (*green dashed curve*) and mean SWDI computed with MWSN records (*red curve*), SAFRAN *(orange)* and WRF + MWSN precipitation (*black curve*), period 1989–2008

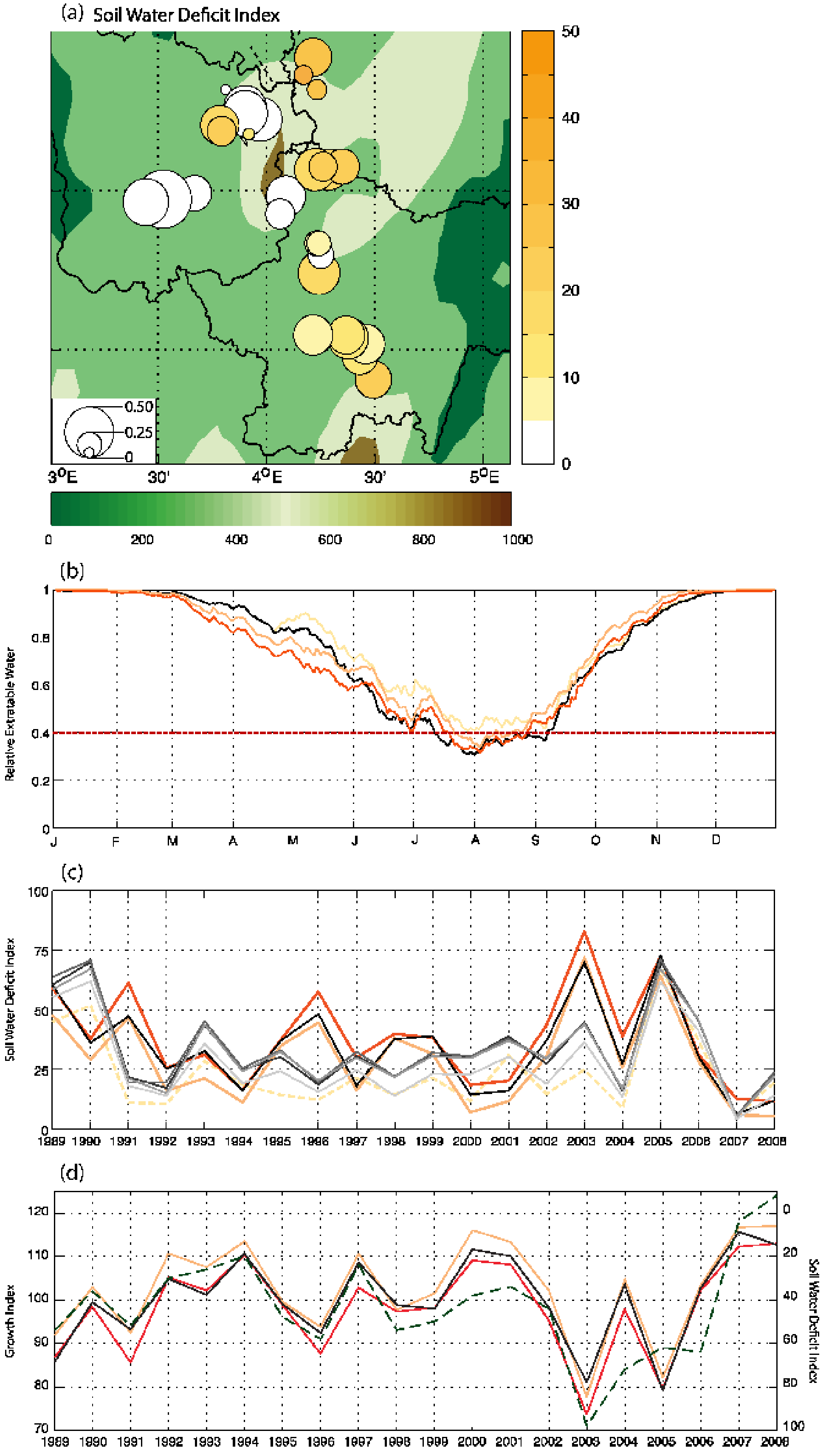

humidity, wind speed, air temperature or solar radiation by observations does not significantly improve the SWDI. The substitution of solar radiation slightly degrades the realism of the SWDI. Thus, the main deficiencies of WRF unambiguously concern its capacity to reproduce at regional scale the precipitation amounts and their seasonality. It is a major difficulty for application in forestry, as the rainfall during the growing season is essential to wood production and tree health.

The interannual variations in the growth index (Sect. 2.5) are negatively correlated with interannual variations in the SWDI (Sergent et al. 2012). In order to evaluate WRF weather variables used to simulated ET_0, three interannual correlations are performed using all stands. The first one is calculated between Douglas-fir growth index and the SWDI (Fig. 15d) computed from the MWSN stations observations, the second one from the SAFRAN data, and the last one merges WRF-simulated climate variables with the MWSN precipitation. Interannual variation in radial growth mirrors the three SWDI at the regional scale. The correlations obtained for the three indexes are highly significant, respectively $r = -0.81$, $r = -0.80$ and $r = -0.77$. In contrast, the correlation coefficient is much lower between the growth index and a SWDI computed from WRF data only ($r = -0.21$, not shown), due to the overestimation of relative extractible water that prevents generating a realistic SWDI.

These results highlight the reliability of the WRF model to simulate weather variables involved in the ET_0 estimation and the low capacity of the model to produce reliable rainfall for relevant impact studies. Although the overestimation of annual precipitation amounts does not exceed 14 % on average (Marteau et al. 2014), the non-stationarity of these biases in space and time (larger during the vegetative season) makes it necessary, to date, to apply a post-correction on simulated precipitation, before using them to feed impact studies.

5 Discussion and conclusion

Accurate estimates of the potential evapotranspiration variability throughout the year and their regionalization are critically important for use in conceptual hydrological, or water balance modelling (Prudhomme and Williamson 2013). The estimation is derived from atmospheric variables such as temperature, wind, humidity and radiation, and could be difficult to obtain for catchments and regions without in situ measurements, or for applications involving future climate projections (Bell et al. 2011). Regional climate models can constitute a potential alternative to scarce observational networks. Nonetheless, their usefulness is questioned by the realism of the simulated climate, especially for precipitation and all the variables used for the computation of ET_0, which are not often considered in climatic studies. Using the state-of-the-art RCM WRF driven by ERA-Interim reanalyses, this study attempted to document the skill of the model for regionalizing all the components used to compute soil water balance, requested for many impact studies. Here, the downscaled results are compared with the SAFRAN analyses, and in situ observations over Burgundy.

The regional simulations reasonably reproduce the spatial distribution of all weather variables. WRF presents lower co-variability with MWSN than ERA-Interim, which assimilates observational data, but significantly reduces its biases for most of the variables. WRF-simulated relative humidity and 2 m-temperature show a clear improvement. Solar radiation and precipitation, especially their spatial patterns, are also fairly well reproduced by the model. WRF reduces some of the biases transmitted by ERA-Interim. Persisting and additional biases are however found in the WRF simulations, including for instance a tendency to overestimate precipitation amounts in spring and summer, a major deficiency for water balance modelling, as well as solar radiation in summer, and the 2 m wind speed in winter.

ET_0 estimated from WRF and SAFRAN outputs show strong discrepancies. However, the WRF simulation is in better agreement than SAFRAN with the ET_0 estimated from the in situ observations. The better geography of WRF solar radiation, in comparison to SAFRAN, may explain most of these discrepancies, since radiation is the dominant variable controlling summer ET_0 (Bois 2007; Ishak et al. 2010).

However, WRF and current climate models more generally, show much stronger limitations for simulating precipitation, especially when convective processes are involved. In this study, the bias in precipitation amounts is close to +14 % regionally, with particularly marked overestimations in summer. Our simulations show too much shortwave radiation reaching the surface and at a same time too much rainfall, suggesting a possible (but indirect) link between precipitation and solar radiation. This may be explained by Alapaty et al. (2012), who have demonstrated that the lack of the subgrid-scale convective cloud-radiation feedbacks in WRF leads to excessive surface radiant energy. In their model, this causes relatively high moist static energy and correspondingly high convective instability, resulting in too frequent activations of parameterized convection. The enhanced surface forcing of convection results in a notable overestimation of precipitation during spring and summer over the US, by about 1–20 mm/day. This missing interaction between cumulus and the radiative budget also affects longwave radiation, and consequently the surface energy budget. This leads thus to strong consequences on temperature and related weather parameters (e.g. relative humidity, pressure) with higher latent heat fluxes. Including subgrid-scale cloud-radiation interactions should improve the simulation of several key climate parameters, the first of which being precipitation. To our knowledge WRF implements this feedback for some cumulus schemes (e.g. Kain-Fritch) since the recent (April 2014) 3.6 release of the model.

In spite of this deficiency in the model's physical package used for this study, the magnitude of the model errors obtained here may be considered in first approximation as satisfactory for geophysical (regional climate) studies. Our results suggest nonetheless that, for impact studies (such as the simulation of soil water availability and for instance its consequences on forest health and productivity), such biases (especially in precipitation amounts) cannot be overlooked, and may require being post-corrected in order to obtain reliable estimators of local-scale bioclimatic conditions.

Future work is thus needed to address more in detail this issue. Numerous studies have already highlighted the efficiency of some statistical/empirical post-processing approaches, such as quantile-mapping (Themeßl et al. 2011; Gudmundsson et al. 2012; Maraun 2013), used to adjust the distribution of modelled data to observed data. Another more elegant, but probably less efficient way at short term, is to improve the simulation of precipitation physically through finer cloud-resolving downscaling exercises. Ultimately, a combination of corrected precipitation and modelled ET_0 may enable us to regionalise drought indexes over the whole region and throughout the century, in order to assess how they will be impacted by climate change.

Acknowledgments The authors thank A. Witterongel, A. Auffray and D. Thevenin, who provided observation data. WRF was provided by the University Corporation for Atmospheric Research website (for more information see http://www.mmm.ucar.edu/wrf/users/download/get_source.html). Biljou© is a web application freely provided by the Forest Ecology and Ecophysiology Unit from INRA (https://appgeodb.nancy.inra.fr/biljou/). Observation records, SATMOS and SAFRAN data were provided by Météo-France. ERA-Interim data were provided by the ECMWF. Calculations were performed using HPC resources from DSI-CCUB, université de Bourgogne Franche Comté.

References

Alapaty K, Herwehe JA, Otte TL, Nolte CG, Bullock OR, Mallard MS, Kain JS, Dudhia J (2012) Introducing subgrid-scale cloud feedbacks to radiation for regional meteorological and climate modeling. Geophys Res Lett 39:L24809. doi:10.1029/2012GL054031

Allen RG, Jensen ME, Wright JL, Burman RD (1989) Operational estimates of reference evaporation. Agron J 81:650–662

Allen RG, Pereira LS, Raes D, Smith M (1998) Crop evapo-transpiration guidelines for computing crop requirements. FAO: Rome. Irrigation and Drainage Paper No. 56

Bell VA, Gedney N, Kay AL, Smith RNB, Jones RG, Moore RJ (2011) Estimating potential evaporation from vegetated surfaces for water management impact assessments using climate model output. J Hydrometeorol 12:1127–1136

Berrisford P, Dee DP, Fielding K, Fuentes M, Kållberg P, Kobayashi S, Uppala SM (2009) The ERA-interim archive. ERA Report Series, No. 1 ECMWF: Reading

Betsch P, Bonal D, Breda N, Montpied P, Peiffer M, Tuzet A, Granier A (2010) Drought effects on water relations in beech: the contribution of exchangeable water reservoirs. Agric Meteorol 151(5):531

Boé J, Terray L, Habets F, Martin E (2007) Statistical and dynamical downscaling of the Seine basin climate for hydro-meteorological studies. Int J Climatol 27:1643–1655

Bois B (2007) Cartographie agroclimatique à méso-échelle : méthodologie et application à la variabilité spatiale du climat en Gironde viticole. Conséquences pour le développement de la vigne et la maturation du raisin. Ph.D. Thesis, Bordeaux, Université de Bordeaux 2, p 211

Boulard D, Pohl B, Crétat J, Vigaud N (2013) Downscaling large-scale climate variability using a regional climate model: the case of ENSO over Southern Africa. Clim Dyn 40:1141–1168. doi:10.1007/s00382-012-1400-6

Bréda N, Huc R, Granier A, Dreyer E (2006) Temperate forest trees and stands under severe drought: a review of ecophysiological responses, adaptation processes and long-term consequences. Ann For Sci 63:625–644

Castel T, Xu Y, Richard Y, Pohl B, Crétat J, Thévenin D, Cuccia C, Bois B, Roucou P, (2010) Assessment of Dynamic downscaling of the continental East French regional climate at high-resolution using the ARW/WRF model, AIC, pp 107–112

Chen F, Dudhia J (2001) Coupling an advanced land-surface/hydrology model with the Penn State/NCAR MM5 modeling- system. Part I: model description and implementation. Mon Weather Rev 129:569–585

Christensen JH, Christensen OB (2007) A summary of the PRUDENCE model projections of changes in European climate by the end of this century. Clim Change 81(Suppl. 1):7–30

Copeland JH, Pilke RA, Kittel TGF (1996) Potential climate impacts of vegetation change: a regional modeling study. J Geophys Res 101:7409–7418

Correia FWS, Alvalá RCS, Manzi AO (2007) Modeling the impacts of land cover change in Amazonia: a regional climate model (RCM) simulation study. Theor Appl Climatol 93:225–244

Crétat J, Pohl B, Richard Y, Drobinski P (2012) Uncertainties in simulating regional climate of Southern Africa: sensitivity to physical parameterizations using WRF. Clim Dyn 38:613–634. doi:10.1007/s00382-011-1055-8

Dee DP, Uppala SM, Simmons AJ, Berrisford P, Poli P, Kobayashi S, Andrae U, Balmaseda MA, Balsamo G, Bauer P, Bechtold P, Beljaars ACM, van de Berg L, Bidlot J, Bormann N, Delsol C, Dragani R, Fuentes M, Geer AJ, Haimberger L, Healy SB, Hersbach H, Holm EV, Isaksen L, Kallberg P, Kohler M, Matricardi M, McNally AP, Monge-Sanz BM, Morcrette J-J, Park B-K, Peubey C, de Rosnay P, Tavolato C, Thepaut J-N, Vitart F (2011) The ERA-Interim reanalysis: configuration and performance of the data assimilation system. Q J R Meteorol Soc 137:553–597. doi:10.1002/qj.828

Droogers P, Allen RG (2002) Estimating reference evapo-transpiration under inaccurate data conditions. Irrig Drain Syst 16:33–45

Dudhia J (1989) Numerical study of convection observed during the winter experiment using a mesoscale two-dimensional model. J Atmos Sci 46:3077–3107

Durand Y (1995) Analyse des principaux paramètres météorologiques de surface sur les massifs alpins et d'autres zones climatiquement homogènes. Technical report, Météo-France. Note scientifique et technique SAFRAN, CEN, Grenoble

Durand Y, Brun E, Mérindol L, Guyomarc'h G, Lesaffre B, Martin E (1993) A meteorological estimation of relevant parameters for snow models. Ann Glaciol 18:65–71

Durand Y, Laternser M, Giraud G, Etchevers P, Lesaffre B, Mérindol L (2009) Reanalyses of 44 years of climate in the French Alps (1958–2002): methodology, model validation, climatology and trends for air temperature and precipitation. J Appl Meteorol Climatol 48:429–449. doi:10.1175/2008JAMC1808.1

Frey-Buness F, Heimann D, Sausen R (1995) A statistical-dynamical downscaling procedure for global climate simulations. Theor Appl Climatol 50(3–4):117–131

Friedl MA, McIver DK, Hodges JCF, Zhang XY, Muchoney D, Strahler AH, Woodcock CE, Gopal S, Schneider A, Cooper A, Baccini A, Gao F, Schaaf C (2002) Global land cover mapping from MODIS: algorithms and early results. Remote Sens Environ 83:287–302

Gandois L, Nicolas M, van der Heijden G, Probst A (2010) The importance of biomass net uptake for a trace metal budget in a forest stand in north-eastern France. Sci Total Environ 408(23):5870–5877

Gautier C, Diak G, Masse S (1980) A simple physical model to estimate incident solar radiation at the surface from GOES satellite data. J Appl Meteorol 19:1005–1012

Gavilan P, Lorite IJ, Tornero S, Berengena J (2006) Regional calibration of Hargreaves equation for estimating reference ET in a semiarid environment. Agric Water Manag 81:257–281

Giorgi F, Mearns LO (1991) Approaches to the simulation of regional climate change: a review. Rev Geophys 29(2):191–216. doi:10.1029/90RG02636

Granier A, Bréda N, Biron P, Villette S (1999) A lumped water balance model to evaluate duration and intensity of drought constraints in forest stands. Ecol Model 116:269–283

Gudmundsson L, Bremnes JB, Haugen JE, Engen Skaugen T (2012) Technical note: downscaling RCM precipitation to the station scale using quantile mapping—a comparison of methods. Hydrol Earth Syst Discuss 9:6185–6201. doi:10.5194/hessd-9-6185-2012

Heck P, Lüthi D, Wernli H, Schär C (2001) Climate impacts of European-scale anthropogenic vegetation changes: a sensitivity study using a regional climate model. J Geophys Res 106(D8):7817–7835. doi:10.1029/2000JD900673

Hong SY, Noh Y, Dudhia J (2006) A new vertical diffusion package with an explicit treatment of entrainment processes. Mon Weather Rev 134:2318–2341

Hutchinson MF (1995) Interpolating mean rainfall using thin plate smoothing splines. Int J Geogr Inf Syst 9:385–403

IPCC (2007) Climate change: synthesis report. In: Pachauri RK, Reisinger A (eds) Contribution of working Groups I, II and III to the fourth assessment report of the intergovernmental panel on climate change. Core Writing Team, IPCC, Geneva, Switzerland

Ishak AM, Bray M, Remesan R, Han D (2010) Estimating reference evapo-transpiration using numerical weather modelling. Hydrol Process 24:3490–3509

Jones C, Giorgi F, Asrar G (2011) The coordinated regional downscaling experiment: CORDEX, an international downscaling link to CMIP5. CLIVAR Exchanges, No. 56, International CLIVAR Project Office, Southampton, UK, pp 34–40

Kain JS (2004) The Kain–Fritsch convective parameterization: an update. J Appl Meteorol 43:170–181

Landman WA, Kgatuke MM, Mbedzi M, Beraki A, Bartman A, du Piesanie A (2009) Performance comparison of some dynamical and empirical downscaling methods for South Africa from a seasonal climate modelling perspective. Int J Climatol 29:1535–1549. doi:10.1002/joc.1766

Laprise R (2008) Regional climate modelling. J Comput Phys 227:3641–3666

Maraun D (2013) Bias correction, quantile mapping, and downscaling: revisiting the inflation issue. J Clim 26:2137–2143. doi:10.1175/JCLI-D-12-00821.1

Maraun D, Wetterhall F, Ireson AM, Chandler RE, Kendon EJ, Widmann M, Brienen S, Rust HW, Sauter T, Themeßl M, Venema VKC, Chun KP, Goodess CM, Jones RG, Onof C, Vrac M, Thiele-Eich I (2010) Precipitation downscaling under climate change: recent developments to bridge the gap between dynamical models and the end user. Rev Geophys 48:RG3003. doi:10.1029/2009RG000314

Marteau R, Richard Y, Pohl B, Chateau Smith C, Castel T (2014) High-resolution rainfall variability simulated by the WRF RCM: application to eastern France. Clim Dyn 44:1093–1107

McAfee SA (2013) Methodological differences in projected potential evapo-transpiration. Clim Change. doi:10.1007/s10584-013-0864-7

Michelot A, Bréda N, Damesin C, Dufrêne E (2012) Differing growth responses to climatic variations and soil water deficits of Fagus sylvatica, Quercus petraea and Pinus sylvestris in a temperate forest. For Ecol Manag 265:161–171

Mlawer E, Taubman S, Brown P, Iacono M, Clough S (1997) Radiative transfer for inhomogeneous atmosphere: RRTM, a validated correlated-k model for the long-wave. J Geophys Res 102:16663–16682

Monteith JL (1981) Evaporation and surface temperature. Q J R Meteorol Soc 107:1–27

Mooney PA, Mulligan FJ, Fealy R (2010) Comparison of ERA-40, ERA-Interim and NCEP/NCAR reanalyses data with observed surface air temperature over Ireland. Int J Climatol 31:487–632. doi:10.1002/joc.2098

Morrison H, Thompson G, Tatarskii V (2009) Impact of cloud microphysics on the development of trailing stratiform precipitation in a simulated squall line: comparison of one- and two- moment schemes. Mon Weather Rev 137:991–1007

Penman HL (1948) Natural evaporation from open water, bare soil and grass. Proc R Soc Lond 193:120–145

Pereira AR (2004) The Priestley–Taylor parameter and the decoupling factor for estimating reference evapo-transpiration. Agric For Meteorol 125:305–313. doi:10.1016/j.agrformet.2004.04.002

Piedallu C, Lebourgeois F, Gégout JC, Seynave I, Vepierre R, Cluzeau C, Nédeltcheva T, Bruno E, Badeau V (2007) Développement, spatialisation, et validation d'indices bioclimatiques. ENGREF-IFN-INRA, p 85

Prudhomme C, Williamson J (2013) Derivation of RCM-driven potential evapo-transpiration for hydrological climate change impact analysis in Great Britain: a comparison of methods and associated uncertainty in future projections. Hydrol Earth Syst Sci 17:1365–1377

Quintana-Seguí P, Le Moigne P, Durand Y, Martin E, Habets F, Baillon M, Canellas C, Franchistéguy L, Morel S (2008) Analysis of near surface atmospheric variables: validation of the SAFRAN analyses over France. J Appl Meteorol Climatol 47:92–107. doi:10.1175/2007JAMC1636.1

Remesan R, Shamim MA, Han D (2008) Model data selection using Gamma test for daily solar radiation estimation. Hydrol Process 22:4301–4309

Rummukainen M (2010) State-of-the-art with regional climate models. WIREs Clim Change 1:82–96. doi:10.1002/wcc.008

Sergent A-S, Rozenberg P, Bréda N (2012) Douglas-Fir is vulnerable to exceptional and recurrent drought episodes and recovers less well on less fertile sites. Ann For Sci 2012:1–12. doi:10.1007/s13595-012-0220-5

Shih SF, Allen LH, Hammond LC, Jones JW, Rogers JS, Smajstrla AG Jr (1983) Basinwide water requirement estimation in southern Florida. Trans ASAE 26(3):760–766

Skamarock WC, Klemp JB, Dudhia J, Gill DO, Barker DM, Duda M, Huang XY, Wang W, Powers JG (2008) A description of the advanced research WRF version 3. NCAR technical note, NCAR/TN\u2013475?STR, p 123

Szczypta C, Calvet JC, Albergel C, Balsamo G, Boussetta S, Carrer D, Lafont S, Meurey C (2011) Verification of the new ECMWF ERA-Interim reanalyses over France. Hydrol Earth Syst Sci 15:647–666

Themeßl M, Gobiet A, Leuprecht A (2011) Empirical-statistical downscaling and error correction of daily precipitation from regional climate models. Int J Climatol 31:1531–1544. doi:10.1002/joc.2168

Van der Heijden G, Legout A, Nicolas M, Ulrich E, Johnson DW, Dambrine E (2011) Long-term sustainability of forest ecosystems on sandstone in the Vosges Mountains (France) facing atmospheric deposition and silvicultural change. For Ecol Manag 261:730–740

Van der Heijden G, Legout A, Pollier B, Bréchet C, Ranger J, Dambrine E (2013) Tracing and modeling preferential flow in a forest soil—potential impact on nutrient leaching. Geoderma 195–196:12–22

Van der Linden P, Mitchell JFB (2009) ENSEMBLES: climate change and its impacts: summary of research and results from the ENSEMBLES project. Met Office Hadley Centre, Exeter

Vautard R, Noël T, Li L, Vrac M, Martin E, Dandin P, Cattiaux J, Joussaume S (2013) Climate variability and trends in downscaled high-resolution simulations and projections over Metropolitan France. Clim Dyn 41(5–6):1419–1437

Vidal JP, Martin E, Franchistéguy L, Baillon M, Soubeyroux JM (2010) A 50-year high-resolution atmospheric reanalyses over France with the Safran system. Int J Climatol 30:1627–1644

Xu CY, Singh VP (2001) Evaluation and generalization of temperature-based methods for calculating evaporation. Hydrol Process 15:305–319

Xu Y, Castel T, Richard Y, Cuccia C, Bois B (2012) Burgundy regional climate change and its potential impact on grapevines. Clim Dyn 39:1613–1626

Zorita E, von Storch H (1999) The analog method as a simple statistical downscaling technique: comparison with more complicated methods. J Clim 12:2474–2489